Pulsed high-density plasmas for advanced dry etching processes

S. Banna, A. Ankargul, G. Cunge, Maxime Darnon, E. Pargon, O. Joubert

REVIEW ARTICLE

Pulsed high-density plasmas for advanced dry etching processes

Samer Banna[a] and Ankur Agarwal
Applied Materials Inc., 974 E. Arques Avenue, M/S 81312, Sunnyvale, California 94085

Gilles Cunge, Maxime Darnon, Erwine Pargon, and Olivier Joubert
CNRS-LTM, 17 rue des Martyrs, 38054 Grenoble Cedex, France

(Received 31 December 2011; accepted 8 April 2012; published 30 May 2012)

Plasma etching processes at the 22 nm technology node and below will have to satisfy multiple stringent scaling requirements of microelectronics fabrication. To satisfy these requirements simultaneously, significant improvements in controlling key plasma parameters are essential. Pulsed plasmas exhibit considerable potential to meet the majority of the scaling challenges, while leveraging the broad expertise developed over the years in conventional continuous wave plasma processing. Comprehending the underlying physics and etching mechanisms in pulsed plasma operation is, however, a complex undertaking; hence the full potential of this strategy has not yet been realized. In this review paper, we first address the general potential of pulsed plasmas for plasma etching processes followed by the dynamics of pulsed plasmas in conventional high-density plasma reactors. The authors reviewed more than 30 years of academic research on pulsed plasmas for microelectronics processing, primarily for silicon and conductor etch applications, highlighting the potential benefits to date and challenges in extending the technology for mass-production. Schemes such as source pulsing, bias pulsing, synchronous pulsing, and others in conventional high-density plasma reactors used in the semiconductor industry have demonstrated greater flexibility in controlling critical plasma parameters such as ion and radical densities, ion energies, and electron temperature. Specifically, plasma pulsing allows for independent control of ion flux and neutral radicals flux to the wafer, which is key to eliminating several feature profile distortions at the nanometer scale. However, such flexibility might also introduce some difficulty in developing new etching processes based on pulsed plasmas. Therefore, the main characteristics of continuous wave plasmas and different pulsing schemes are compared to provide guidelines for implementing different schemes in advanced plasma etching processes based on results from a particularly challenging etch process in an industrial reactor.
[http://dx.doi.org/10.1116/1.4716176]

I. INTRODUCTION

A. Plasma etching in semiconductor manufacturing

Since the early 1980 s, plasma etching has been an indispensable tool in the semiconductor manufacturing industry to precisely transfer mask patterns, defined by lithographic resist, to underlying layers of solid material.[1] Plasma etching offers a unique way to modify surface properties of materials using reactive species created in the gas phase. Rates for the gas-phase chemical reactions are governed by plasma properties such as electron and ion densities and electron temperature, while the flux and energy of the ions and radicals incident on the surface govern surface reaction rates.[1] Due to the complexity associated with plasma etching, the exact etching surface mechanisms are difficult to determine. The complexity arises partly from the multiplicity of gas-phase reaction pathways (e.g., excitation, ionization, dissociation, attachment, recombination), which affects the concentrations of active precursors (both charged and neutral species) and depends on the feedstock chemistry, discharge configuration, characteristics of chamber wall materials, gas and surface temperatures, and operating parameters (pressure, flow rates, etc.).

As device feature size shrinks, many process requirements become more stringent. These include higher selectivity (defined as the ratio of etch rates of the film and substrate, or the film and photoresist or other materials used as a mask), more anisotropic etch (i.e., vertical etch rate must greatly exceed the lateral etch rate), tighter critical dimension control, reduced plasma induced damage, and superior throughput. Controlling plasma properties in a dry etching reactor is essential to meet these challenging requirements for devices at and beyond the 22 nm technology node. Critical factors affecting overall on-wafer performance during plasma etching processes for advanced technologies are uniformity at both macroscopic (i.e., wafer) and microscopic (i.e., die) levels, etching versus deposition, vertical versus lateral etch

[a]Author to whom correspondence should be addressed; electronic mail: samer_banna@amat.com

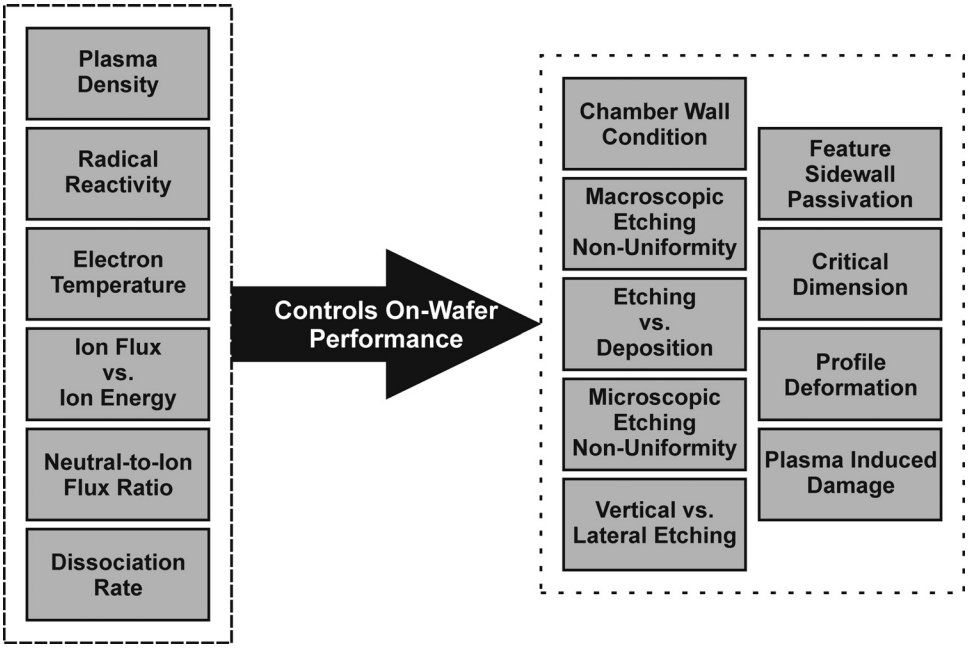

FIG. 1. Control challenges for advanced dry etching processes. The left half lists the critical plasma characteristics that need to be controlled to achieve optimal on-wafer performance as characterized by aspects/parameters outlined in the right half.

rate, profile control, reactor wall conditioning and cleaning, feature sidewall passivation, and plasma induced damage, as shown schematically in the right half of Fig. 1. The left half of Fig. 1 details the important plasma parameters governing control of these factors (i.e., plasma density, reactivity of radicals, electron temperature, ion flux and energies, neutral-to-ion flux ratio, and dissociation rate).

Fulfilling the challenges noted above relies in large part on independent control of these plasma parameters. Unfortunately, in conventional plasma processing, requirements and performance-determining factors frequently conflict and may be difficult to reconcile simultaneously given the absence of specific controls. Hence, achieving the desired on-wafer performance to meet the technology challenges might be limited and is, at best, a trade-off. Thus, there is a vital need for wider and more flexible ranges of plasma operating conditions to improve etch process control. This limitation has triggered extensive research among the academic and industrial communities to identify new approaches and methods for the design and control of the next generation of plasma processing reactors.

B. High-density plasmas for etching processes

For the past two decades, high-density plasmas (HDPs), such as electron cyclotron resonance (ECR) plasmas, helicon wave plasmas, and inductively coupled plasmas (ICPs), have been widely used in etching processes to meet some of the previously listed challenges and to achieve flexible plasma control.[1–3] (Note that while capacitively coupled plasma sources are equally capable of producing high plasma densities, the major focus of this review is on inductively coupled plasma sources.) In such plasmas, radio-frequency (RF) (as used in ICP) or microwave (as used in ECR or helicon wave plasmas) power is coupled to the plasma across a dielectric window rather than by a direct connection to an electrode in the plasma reactor as is the case in capacitively coupled plasmas (CCPs). Typical industrial ICP sources operate at 13.56 MHz, while ECRs typically operate at 2.45 GHz. This method of power transfer is the key to achieving high plasma densities with low voltages across all plasma sheaths at electrode and wall surfaces. Hence ion acceleration energies are typically on the order of the plasma potential (i.e., 15–30 eV).[1–3] In such plasmas, the ion energy is controlled by an independent RF power supply capacitively coupled to the substrate electrode by varying the bias voltage at the wafer level. Thus, unlike CCP plasmas, HDPs provide *almost* independent control of the ion flux and ion energies incident on the wafer. Conventional industrial HDP reactors utilize RF frequencies for the bias ranging from 400 kHz to 60 MHz.[2,3] Such HDPs have been able to efficiently provide the radicals and ions required for etching processes to fabricate ultra-large-scale integrated circuits.

The challenge to define a finer pitch while maintaining high productivity in fabrication has driven the dry etching process regime in HDPs toward lower pressures and higher plasma densities, which significantly increases the directionality and anisotropy of positive ions incident on the wafer.[4] The general trends for the process operational regimes (pressure and plasma density) for typical dry etching applications are shown in Fig. 2. In the low pressure, high plasma density regime, ionization ratios are higher and the ion energies are more controllable. However, potential plasma induced damage (PID) poses a risk to device performance when operating in this regime. PID can occur in one or more of the following forms:

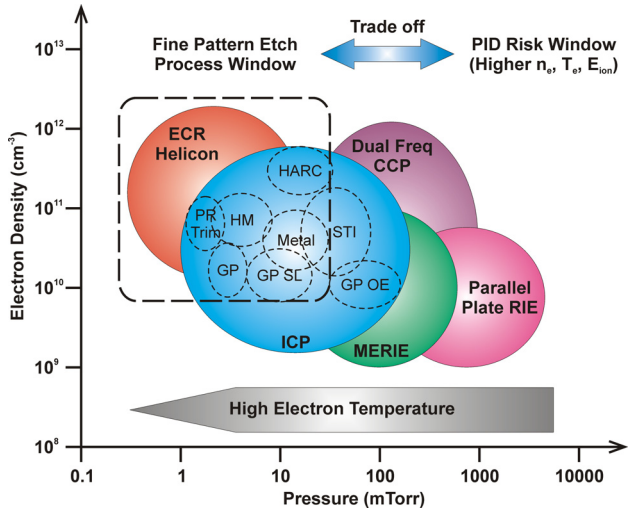

FIG. 2. (Color online) Typical regimes of operation for different dry etching applications as a function of plasma density and operating pressure (adapted from Ref. 4). Acronyms key: ECR—electron cyclotron resonance, PR—photo resist, HM—hard mask, GP—gate poly, OE—over etch, SL—soft landing, HARC—high aspect ratio contact, ICP—inductively coupled plasma, CCP—capacitively coupled plasma, RIE—reactive ion etching, MERIE—magnetically enhanced RIE.

(1) Surface physical damage from highly energetic ions bombarding the wafer.
(2) Photon bombardment from high ultraviolet (UV) and vacuum ultraviolet (VUV) radiation during plasma operation in HDPs.
(3) Plasma nonuniformity induced charging arising from spatial nonuniformity[5–7] in the plasma potential and subsequent spatial nonuniformity in the surface potential on the wafer. The nonuniform surface potential distribution can force tunneling currents to flow through thin gate oxides, causing damage, or cause local charging of island structures, distorting ion trajectories and etch profiles.
(4) Differential charging due to negative charging at the top of the high aspect ratio features by the isotropic flux of plasma electrons and positive charging at the bottom by the directed flux of plasma ions.

The impact of PID on the overall device performance manifests itself in either one or more of the following:[5–14]

(1) Degradation of electrical performance of the device from defects that compromise gate oxide integrity, leading to a lower breakdown voltage of a metal-oxide-semiconductor (MOS) capacitor or a significant threshold voltage shift in a MOS transistor.
(2) Differential charging or electron shading[9] that might distort etch profiles and induce catastrophic tunneling currents through the thin gate oxides, also eventually leading to a shift in the breakdown and threshold voltages.

A potential method for mitigating PID is the use of time-modulated plasmas for advanced dry etching processes. This is because:

(1) Time-modulated plasma, in general, exhibits lower effective electron temperature and plasma density.[15–19]
(2) Under certain time-modulation configurations—synchronous pulsing in particular (see below)—the plasma sheath might collapse, allowing charge relaxation and subsequent reduction in charge imbalance.[4,18–21]
(3) Flexible control of the ion energy distribution function (IEDF) allows operation with lower average ion energy while etching.[4,15,19,22,23]
(4) Minimization of UV radiation dose helps reduce UV radiation damage while surfaces are exposed to plasma during processing.[24,25]
(5) It permits flexible control of ion flux composition as molecular ions dominate during time-modulated plasma while atomic ions dominate during continuous mode operation.

C. Continuous versus time-modulated power coupling

Conventional ICP reactors use an RF power source with *constant* average power or voltage to excite plasma in a vacuum chamber. This is known as the *continuous wave* (CW) RF mode. Over the past three decades, several researchers have demonstrated through both experimental studies and computational investigations that time-modulated RF power input, i.e., *pulsed* RF mode, can increase the plasma processing flexibility by enlarging the range of operating conditions for stable plasma operation.[22] Two main parameters characterize the RF pulse: *pulse frequency*, i.e., the frequency at which the RF power is turned on and off per second, and *pulse duty cycle*. The latter is defined as the ratio between the pulse on-time and the total pulse duration. By varying the pulse frequency and duty cycle, pulsed plasmas provide additional "tunable knobs" through which primary plasma properties such as ion/electron densities, electron temperature, ion/neutral flux ratio, plasma dissociation, and plasma potential can be controlled.[22]

Pulsed plasmas were first investigated in the late 1980 s at multiple research laboratories with the aim of understanding the fundamentals of plasma physics. Along with these investigations,[15,26–36] pulsed plasmas were evaluated for etching a wide range of materials used in microelectronics (semiconductor, conductor, insulator, and magnetic materials) and showed great promise for solving typical issues faced during an etching process. For example, pulsed plasmas have been utilized for gate patterning applications to achieve highly selective, highly anisotropic, notch-free (local side etching) polycrystalline silicon etching with no charge build-up damage.[15,26–30] One type of PID (differential charging in features due to electron shading) that leads to undesirable profile distortions during etching (e.g., micro-trenching, bowing, and notching) may also be mitigated by using pulsed plasmas.[22] During the after-glow phase (power-off period), low-energy ions with broader angular distribution help neutralize the differential charge. Further, it has been suggested that negative ions can be injected into the feature to neutralize charge deposition by positive ions during the after-glow phase during which the typical electron-ion plasma transitions to ion-ion plasma in an electronegative gas mixture.[31–35]

Another type of PID (ultraviolet radiation damage) has also been shown to decrease when using pulsed RF.[19,24,25] Pulsed plasmas have also gained recognition as a means of controlling the plasma deposition environment.[36]

Despite successful demonstrations of pulsed plasmas, interest from the industrial community had been weak until recently due to repeatability concerns.[4,22] Indeed, the continued shrinking of CMOS devices requires the development of more complex plasma etching processes with the ability to control patterning performance at the nanometer scale. Moreover, there are limitations to patterning complex stacks of very thin layers without damage using conventional CW plasmas. Accordingly, the challenge in accurately defining the pattern over the wafer at the nanometer scale is growing. In particular, selective etching of ultra-thin layers without damaging the underlying layer is getting progressively difficult to achieve, as the lowest energy of the ion flux impinging the surface in CW plasmas is at least 15–30 eV (based on the sheath potential at a floating wall). Ions in this energy range can damage materials up to a depth range of 1–2 nm, which is unacceptable, for example, for thin silicon-on-insulator (SOI) film processing. As novel device structures (e.g., FinFETs—fin-shaped field effect transistors) employ new materials that are either extremely thin and fragile (Graphene) or difficult to etch (metal oxides), the challenges are expected to be of greater complexity.

During the past 5 years, major hardware changes in the design of plasma reactors have led to some improvements but have only a limited effect on the direct control of plasma properties. Pulsed plasma technologies are among the very few technologies that enable superior control of plasma properties with only a minor change in hardware. Certainly, pulsed plasma offers new tuning knobs (pulse frequency, duty cycle, and optional phase lag between source and bias pulses) that enhance independent control of plasma conditions (in particular, ion bombardment energy and plasma chemical composition) otherwise difficult in continuous wave plasmas. Several pulsing modes can be envisaged. For example, either only the source or the bias generator is pulsed (hereafter referred to as source pulsing and bias pulsing, respectively); both bias and source are simultaneously pulsed (synchronous pulsing) with or without time delay between them. Since power is actively deposited for only a fraction of the time, pulsed plasmas offer the possibility of working with low ion energy regimes (below 5 eV) and with less dissociated (and less reactive) plasmas, resulting in a better process performance in terms of damage, selectivity, and profile control.

D. From academic research to industrial manufacturing

The lack of efficient and stable coupling of pulsed RF power has substantially limited the operating window; thus allowing for only a very limited number of applications in mass production.[4,22,37] Pulsed RF power has commonly been coupled in ICP reactors using one of two methods. One is "bias pulsing" wherein the ICP source is operated in CW RF mode while the biased substrate is in pulsed RF mode. In contrast, the ICP source is pulsed during "source pulsing" in the presence of a CW RF substrate bias.

The main challenge with either method is managing the amount of reflected power, i.e., ensuring efficient power transfer to the plasma while pulsing. In ICP reactors specifically, a high reflected bias power is observed in low-pressure processes (a few tens of mTorr and below) with source pulsing, in which the time-modulation of the source power is highly coupled to the bias. The high reflected power is attributed mainly to the nature of pulsed plasma, as the plasma impedance varies rapidly within the pulse. Typical pulse durations are on the order of tens to hundreds of microseconds. These rapid variations cannot be tracked by a conventional commercial dynamic matching network due to the mechanical nature of its adjustment. The response time of such an adjustment is at best on the order of tens of milliseconds. Therefore, for pulse frequencies greater than 1 kHz (i.e., a pulse duration of less than 1000 μs), high reflected power might occur. Even if the RF source were to operate in a "load power" mode when the source would compensate for the reflected power, there are repeatability and reliability concerns while operating with very high (>20%) reflected power.

These RF power coupling challenges highlight the need for production-worthy pulsed plasma technology. Hence, the development focused on technology to improve RF power delivery when in pulse mode at the sub-millisecond scale. During the past few years, multiple techniques were proposed to reduce reflected power and ensure more efficient power delivery during pulsed plasma operation. In their invention, Todorow *et al.*[38] proposed to hold the variable capacitors, typically used in a matching network, at a constant position during pulsed plasma operation. The positions at which the capacitors are held are determined based on the CW operation for similar plasma conditions used prior to the transition to the pulsed mode. In such a scenario, it is assumed that the tuning positions of the matching network during the active glow (power-on period) phase are similar to the CW. However, during the after-glow (power-off period) phase the positions at which the capacitors are held might provide poor RF matching under certain pulse conditions. Accordingly, the source pulsing window of operation utilizing such a scheme might be limited,[4] although still better than that achieved when the capacitors are not held at a constant position and are constantly trying to tune.

Another technique for tuning RF power delivery during pulsed plasma is frequency tuning,[39] so called because the operating frequency of the RF power is modulated around the fundamental frequency, allowing impedance matching. The main advantage of this approach is that the tuning algorithm is extremely fast and capable of tracking rapid changes within the pulse; thus facilitating suppression of reflected power. Nevertheless, typical industrial RF power supplies operating at 13.56 MHz provide only a limited range for frequency tuning of $\pm 5\%$ at best. In their invention, Banna *et al.*[40] proposed a time-resolved approach to further enlarge the window of operation with pulsed plasma. They suggested

combining both of the aforementioned inventions so that the matching network tunes RF power delivery on the longer time scale while utilizing frequency tuning over shorter time scales. Furthermore, rather than holding the match tuning positions based on CW operation, they proposed that the positions be held based on a pulsed plasma operating at 90% duty cycle prior to the transition to the desired duty cycle for which the frequency tuning kicks in. Banna *et al.*[22] demonstrated that by utilizing this technique the pulsed plasma window of operation can be significantly improved (see Tables I–V in Ref. 22).

Utilizing the above techniques, commercial 300 mm ICP silicon etch tools have become available that fully support the operation of pulsed plasma with a wider window of operation and better RF power delivery management.[22] The impedance matching response time is reduced to a few microseconds, ensuring a low level of reflected power acceptable for a wide variety of applications. In fact, in addition to the source- and bias-pulsing modes of operation, these tools also feature the capability to simultaneously pulse both source and bias powers, also known as synchronous pulsing. In this synchronous mode of operation, the ICP source and substrate bias are pulsed at the same frequency and duty cycle, and can be operated with or without phase delay between their respective pulses. Recently, another pulsing scheme was introduced, wherein both source and bias are synchronized at the same pulse frequency but with different duty cycles, making it possible to "embed" the bias pulse within the source pulse if the powers are pulsed with a time delay between them.[41]

E. Fundamentals of pulsed plasma

Pulsed plasmas introduce new regimes relative to CW plasmas owing to new parameters, specifically the pulse frequency and the pulse duty cycle. In contrast to CW operation, wherein the plasma attains a quasi-steady state, the plasma is truly transient in a pulsed operation. In Fig. 3, various regimes and their impact on basic plasma properties in pulsed plasma are shown. Plasma properties, such as electron temperature, electron and ion densities (as a result of the impact on ionization rates), and plasma potential, vary depending on the duty cycle, on the order of the pulse frequency (time-scale of tens to thousands of microseconds). The period during which power is deposited (qualified by duty cycle) is referred to as the "active-glow"; after-glow refers to the period when no power is deposited. However, as described below, plasma properties differ during the "initial" active- and after-glow periods compared to the "steady-state" active- and after-glow periods. For the purpose of this discussion, we assume that the pulse modulates the "source" power, i.e., power deposition governs primarily plasma generation and not ion acceleration toward a substrate.

1. Initial active-glow period

As power is momentarily turned on, the plasma ignites and the electron (and ion) density starts to rise, but does not quite attain a steady state. This also coincides with the formation of the sheath near all surfaces. Since the power deposition is at its peak value and the electron density is low, the average electron energy (i.e., the electron temperature) during this period is initially high. Consequently, the plasma potential and ion energies are also high. However, if the initial plasma density at the beginning of the pulse is negligible (following a long after-glow period), the low ion density during this period results in a low ion flux density to the surfaces.

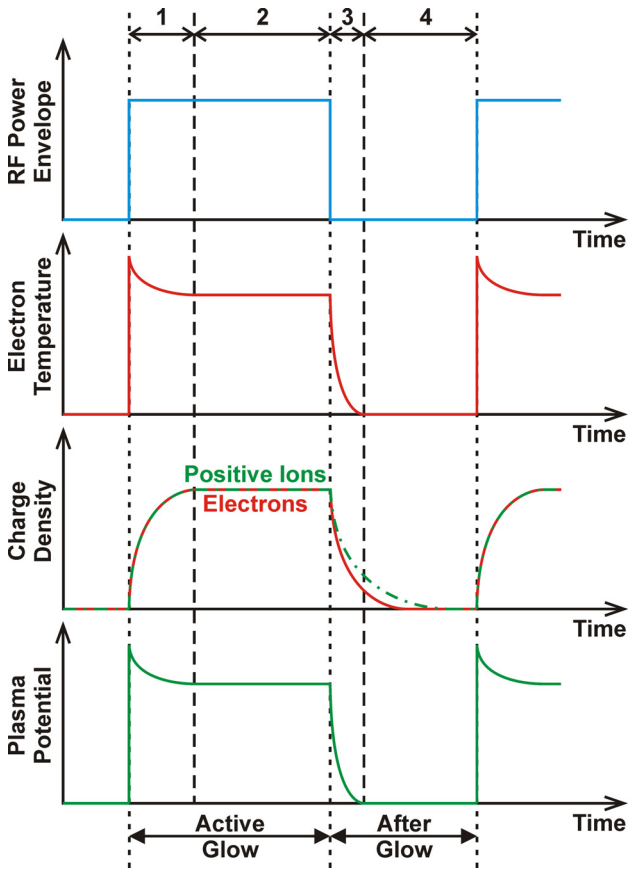

FIG. 3. (Color online) Time modulation of the RF power envelope, electron temperature, density of positive ions and electrons, and the plasma potential during pulsed plasma operation. Region 1 refers to the initial active-glow period, 2 refers to the steady-state active-glow period, 3 refers to the initial after-glow period, and 4 refers to the late after-glow period.

2. Steady-state active-glow period

This regime is, in principle, not any different from the steady-state CW plasma. As the plasma transitions to the steady-state active-glow period, the electron and ion densities attain steady-state values. Electron temperature and plasma potential also attain steady-state with values commensurate with those observed during CW operation. This period is characterized by high ion flux and almost constant plasma impedance. Note that this phase might not be achieved for high pulse frequencies and low duty cycles for which the transitional phase is dominant.

3. Initial after-glow period

As power deposition is momentarily turned off, the inductive electric fields responsible for electron heating decrease

rapidly. As the electrons are no longer heated, they dissipate their energy in collisions and by escaping to the walls (overcoming the smaller sheath potentials), and the electron temperature (T_e) drops very rapidly during this period. The plasma potential, which is commensurate with T_e, also starts decreasing rapidly and the sheath begins to collapse accordingly. At the same time, electron and positive ions are transported to (and recombined on) the surfaces by ambipolar diffusion and their density decays at a slower rate than T_e. In thermally attaching electronegative gases (Cl_2, SF_6, etc.) electron attachment is enhanced at low T_e, leading to the formation of negative ions that further enhances electron loss (and leads to an increase in negative ion density). Both ion flux and ion energy drop rapidly during this period.

4. Late after-glow period

By the time the plasma transitions to this regime, electron density is at its lowest levels with close to thermal energies only. In general, the level to which the plasma density drops depends on the duty cycle and the pulse frequency. The larger the duty cycle and pulsing frequency the shorter the after-glow period, resulting in only small losses. If the pulse frequency is low, the after-glow period is long (even for large duty cycles), resulting in greater depletion of the charged species. In electronegative discharges, plasma transitions to an ion/ion (i.e., positive and negative ions) state as the dominant negatively charged species are the negative ions and not electrons. As the mobilities of the positively and negatively charged species are similar, the sheath is typically thin under such conditions.

Note that the above descriptions assume lack of any capacitive power (bias power) for ion acceleration. The dynamics during the after-glow period is significantly influenced in the presence of such an RF bias. For example, the lower ion and electron fluxes result in a higher voltage for a constant power, leading to not only thicker sheaths but also capacitive heating of electrons; consequently, a higher electron temperature. Further, if only the bias power is pulsed instead of the source power, the dynamics of bulk plasma characteristics do not apply and the characteristics of ion energy and angular distribution (IEAD) functions are dominantly affected. The consequences of pulsing on IEADs in the presence of an RF bias are discussed later.

In the absence of an RF bias the ions, bombarding the wafer, do so with energies approaching the plasma potential during the pulse (15–30 eV in the active-glow period and approximately 1 eV during the after-glow period). The time-averaged ion energy distribution function can be varied to be dominant at, for example, 15 eV versus 1 eV by adjusting the duty cycle of the pulse, as shown schematically in Fig. 4(a). Furthermore, during the late after-glow period, as the sheath has collapsed, the angular distribution of the ions incident on the wafer is broad, which facilitates charge neutralization near the top of the feature being etched. Additionally, the collapsed sheath during this phase of the pulse may allow negative ions to reach the bottom of the feature, as shown in Fig. 4(b), thereby reducing the positive charge build-up. Finally, owing to the fast electron temperature decay in the after-glow, the electron impact dissociation reaction rates drop rapidly, which significantly reduces radical production. At the same time, radicals are lost on the reactor walls where they stick or recombine and their density decays in the after-glow. However, as discussed later, the typical time to achieve any significant radical density variation is on the order of several milliseconds, i.e., much longer than the pulsing period (even at a pulsing frequency of 1 kHz) over which ion flux and ion energy vary. Under such conditions, the ion flux is rapidly modulated while the radical flux is constant and independent of the duty cycle. This is why plasma pulsing at high frequencies allows an almost independent control of the ion flux and radical flux to the wafer.

F. Review outline

The review is organized as follows: In Sec. II, the characteristics of pulsed HDPs are reviewed based on multiple diagnostic techniques and computational models employed at various research laboratories across the world. In particular, the dynamics of charged and neutral species under different pulse conditions are reviewed. Section III focuses on the use of pulsed plasmas for applications before widespread industry adoption, specifically in etching conductor, magnetic, and dielectric materials.

Section IV uses various examples to trace implementation of pulsed ICPs in industrial reactors for advanced dry etching processes. The impact of pulsed plasmas on etching rate selectivity and uniformity, profile control, and other parameters is discussed. The impact of pulsed plasmas on pattern transfer, profile evolution, and passivation control are discussed for shallow trench isolation (STI) etching processes. Section V addresses future directions and challenges in utilizing pulsed ICPs, followed by a brief summary and concluding remarks.

II. CHARACTERISTICS OF PULSED PLASMAS

Modulation of power in HDP sources has important consequences not only on the charged species densities and fluxes but also on the plasma chemistry. The impact of power modulation on plasma properties has been investigated both experimentally, utilizing different plasma diagnostic tools, and via a variety of computational models established over the past two decades. This section discusses separately the effect on kinetics of charged species and neutral radicals. The dynamics of high density plasma systems are governed primarily by the source power. However, as most industrial plasmas of interest also apply an RF bias to the wafer, the dynamics of charged species can be different compared to when no RF bias is applied. In particular, the characteristics of IEDFs are modulated in pulsed plasmas in the presence of bias. To that end, we separately discuss the characteristics of pulsed plasmas in the presence of a substrate bias. This is followed by discussing the impact of pulsed plasmas on the IEDF and the dynamics of radicals while time-modulating the plasma.

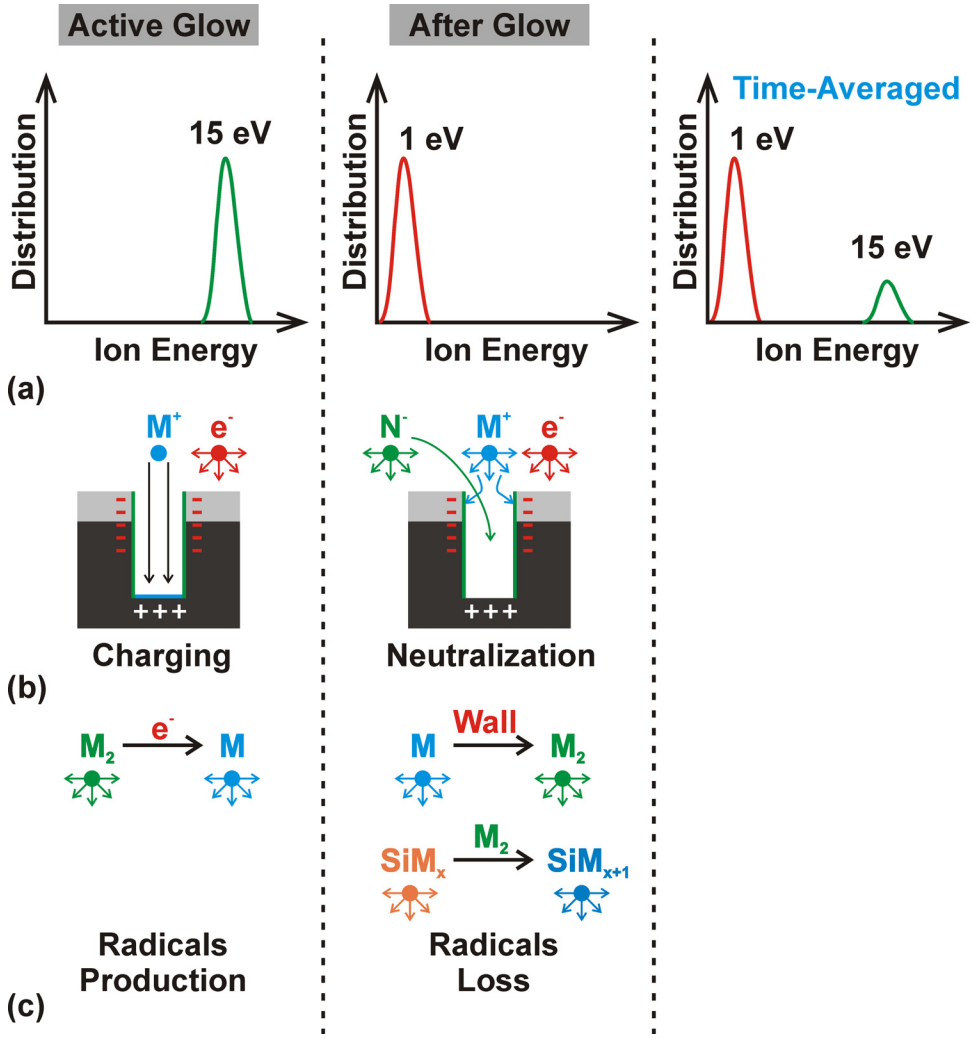

FIG. 4. (Color online) Schematic of (a) ion energy distribution, (b) charge distribution on the feature, and (c) radicals production and loss mechanisms during the active-glow and after-glow periods in pulsed plasma operation.

A. Dynamics in the absence of substrate bias

1. *Electropositive plasmas*

The physics of pulsed Ar discharges has been investigated using computational models of varying dimensionality from zero- through three-dimensions. For example, Ashida *et al.*[42] investigated the temporal characteristics using volume-averaged global models while Lymberopoulos *et al.*[43] used a one-dimensional fluid model to investigate the spatial and temporal dynamics. Two- and three-dimensional fluid computational investigations of pulsed ICPs in Ar were reported by Subramonium and Kushner.[44,45] Overall, similar conclusions were drawn from models of varying complexity. For example, the temporal dynamics of the reactor averaged electron density, n_e, and electron temperature, T_e, are shown in Fig. 5, in an Ar plasma for a peak power of 500 W, pulsed at 10 kHz, with duty cycles of 30%–70% as reported by Subramonium and Kushner[45] using their three-dimensional hybrid model. Electron temperature rises rapidly at the beginning of the active-glow period, resulting in a small over-shoot before reaching a quasi-steady-state value. During the after-glow period, T_e drops rapidly in about 10 μs, irrespective of the duty cycle. As the peak power is maintained constant, the time-averaged power deposition increases with duty cycle, leading to an increase in the reactor-averaged n_e (and hence, the positive ion density) at the end of the active-glow with duty cycle. Upon termination of power, electron density decays due to ambipolar diffusion and recombination on the walls, but over longer time scales (several tens of microseconds).

The volume-averaged global model by Lieberman and Ashida[46] provides some insight into the physics behind these time scales. The results of Subramonium and Kushner[45] are in excellent agreement with the global model in Ref. 46. The global model solves the set of differential equations governing the densities and energy of the charged species (and radicals). The transient behavior of the plasma density is obtained by the particle balance equation:

$$\frac{1}{n_e}\frac{dn_e}{dt} = \nu_{iz} - \nu_{\text{loss}}, \tag{1}$$

where $\nu_{iz} = k_{iz} n_g$ is the ionization rate and $\nu_{\text{loss}} = u_B / l_{\text{eff}}$ is the characteristic particle loss rate on the reactor walls. Note that u_B is the Bohm velocity, l_{eff} is the effective reactor size,

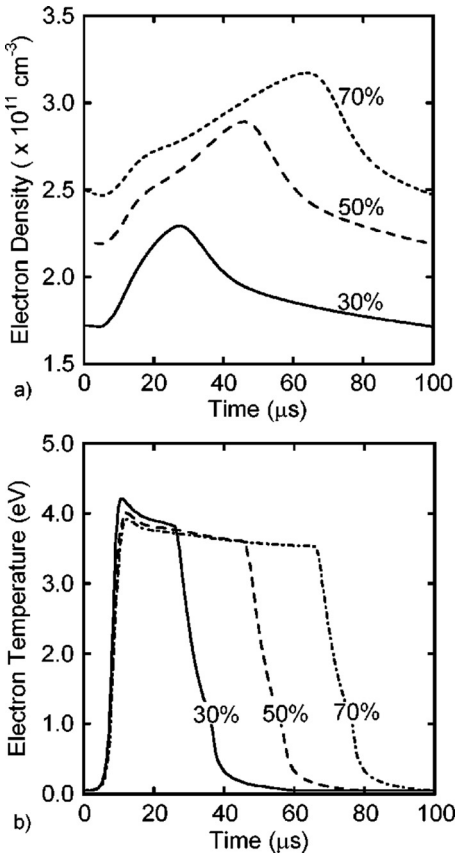

FIG. 5. Temporal dynamics of (a) electron density and (b) electron temperature in Ar plasma with a peak ICP power of 500 W pulsed at 10 kHz for duty cycles of 30%–70%. Reprinted with permission from P. Subramonium and M. J. Kushner, J. Appl. Phys. **96**, 82 (2004). Copyright 2004, American Institute of Physics.

k_{iz} is the ionization rate, and n_g is the gas density. As such, ν_{iz} varies exponentially with T_e while ν_{loss} varies as the square root of T_e. Lieberman and Ashida[46] showed that in the active-glow period, Eq. (1), has the solution

$$n_e(t) \approx n_{emin} + (n_{e\infty} - n_{emin})e^{-\nu_\infty t}, \tag{2}$$

where n_{emin} is the electron density at the beginning of the pulse, $n_{e\infty}$ is the steady state electron density and ν_∞ is the ionization rate in the steady state plasma. For a steady state T_e of 3 eV in Ar at 5 mTorr, $\nu_\infty = 3 \times 10^{-4}$ s^{-1} that yields a rise time for the electron density of 35 μs. The temporal variations of T_e are obtained from an energy balance [Ref. 46, Eq. (17)]. However, there is no simple analytical solution to describe the rise of T_e at the beginning of the pulse. On the other hand, it is possible to estimate the amplitude of the overshoot in T_e [Ref. 46, Eq. (20)], which is commonly observed in pulsed plasmas. This peak in T_e is a consequence of the power dissipation into a smaller inventory of electrons that survives at the end of the after-glow of the previous pulse. The overshoot in the initial active-glow in T_e is usually small (except for prolonged after-glow periods) compared to electronegative plasmas, the implications of which are discussed later.

The analytical expressions representing the decay rate of both n_e and T_e during the after-glow phase are

$$T_e(t) \approx T_{e\infty}[1 + 2\nu_\infty(t - \alpha\tau)]^{-2}, \tag{3}$$

$$n_e(t) \approx n_{e\max}[1 + 2\nu_\infty(t - \alpha\tau)]^{-0.5}, \tag{4}$$

where α is the duty cycle, τ is the pulse period, $T_{e\infty}$ is the steady state electron temperature, and $n_{e\max}$ is the electron density at the end of the pulse period. Note that at steady state, the left-hand side of Eq. (1) will be zero and so $\nu_\infty = k_{iz}n_g = u_B/l_{\text{eff}}$ is the effective loss rate of charged species on the reactor walls. From Eq. (3), in the after-glow, electron temperature decreases mostly due to the loss of electron kinetic energy on the reactor walls. Note that the electron energy loss via inelastic collisions is significant only in the early after-glow when $T_e > 1$ eV since ionization of Ar atoms have a threshold energy of 15.6 eV.[47] Measurements of Sugai *et al.*[48] indicate that the time scales as predicted by the global models are highly accurate.

The decay of electron density also occurs over a time scale determined by the loss rate of charged particles on the walls, which in a volume-averaged global model is assumed to be in equilibrium with the plasma potential. As such, the decay of electron density is determined by the ambipolar diffusion loss of ions to the walls. In the after-glow, this rate decreases with time as a result of electron cooling.[44] However, Eqs. (2)–(4) accurately capture the dynamics of electron density and temperature in the after-glow and were found to be in good agreement with the Langmuir probe based experimental measurements.[46,47]

2. Electronegative plasmas

Characterization of discharges sustained in electronegative gases, such as SF_6, Cl_2, CF_4, etc., is complicated by the presence of negative ions. Negative ions modify the charged particle transport coefficients as ambipolar diffusion takes place between negatively charged species (electrons and low-mobility negative ions) and positive ions. Typically, the positive ion Bohm flux to the surfaces is reduced in the presence of negative ions. However, in the active-glow, the relatively cool negative ions are typically confined to the plasma bulk by the plasma potential and do not reach surfaces. Extensive experimental studies have been conducted of electronegative pulsed plasma dynamics in Cl_2,[20,35,49,50] CF_4,[51] and O_2 (Refs. 52 and 53) plasmas. Computationally, pulsed Cl_2 discharge is the most often characterized via Monte Carlo simulation[18] and zero-,[54–56] one-,[57] two-,[44,58,59] and three-dimensional[45] models. Discharges sustained in O_2,[60,61] SF_6,[62,63] and CF_4 (Ref. 55) have also been computationally investigated. In general, there is good agreement between the computational investigations and the experimental studies of pulsed electronegative discharges.

The temporal dynamics of the reactor-averaged densities of electrons and Cl^- and electron temperature in a Cl_2 plasma for a peak power of 300 W, pulsed at 10 kHz with varying duty cycles of 30%–70% are shown in Fig. 6.[45] Since Cl_2 is a thermally attaching molecule, the mechanism of negative ion formation by dissociative attachment processes has its peak cross-section at low electron temperatures. During the

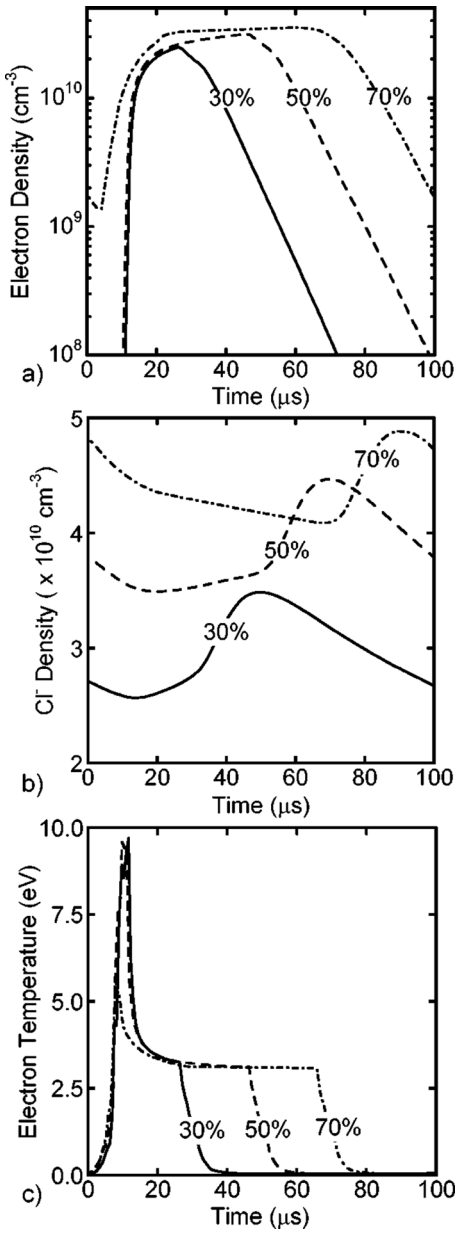

FIG. 6. Temporal dynamics of (a) electron density, (b) Cl^- density and (c) electron temperature in Cl_2 plasma with a peak ICP power of 300 W pulsed at 10 kHz for duty cycles of 30%–70%. Reprinted with permission from P. Subramonium and M. J. Kushner, J. Appl. Phys. **96**, 82 (2004). Copyright 2004, American Institute of Physics.

after-glow period, when electron temperature decreases, more electrons are lost via attachment processes, leading to negative ion formation and a faster electron density decay rate than in electropositive plasma. This increase in loss rate of electrons during the after-glow period (compared to Ar plasma) has also been observed experimentally.[20] An important consequence of the additional electron loss mechanism in electronegative discharge is the markedly higher overshoot in electron temperature at the beginning of the active-glow. As such, an E-to-H mode (capacitive to inductive coupling dominated mode) jump may also be observed during the initial active-glow of a pulse due to the prohibitively large drop in electron density during the after-glow as may be the case at lower duty cycles or low pulse frequencies.[51] In the active-glow period, the density of Cl^- typically decreases due to the decrease in attachment rate and an increase in ion-ion neutralization (due to greater ionization) as a consequence of the rise in electron temperature. Finally, the density of Cl^- in the after-glow period does not increase monotonically as the production rate is limited by the availability of electrons. As the electron density decreases to very low levels, Cl^- production saturates, yielding ion-ion plasma. The Cl^- density subsequently decreases due to ion-ion recombination processes and diffusion losses at the walls.

The formation of ion-ion plasma in the late after-glow has also been observed experimentally and is of considerable interest.[35,49,51] In such a plasma, negative ions are not necessarily confined to the potential well and, therefore, can presumably facilitate neutralization of charge buildup in features on the wafer. (Note that there is some debate as to the role of negative ions in reducing differential charging.[14] In particular, low-energy positive ions have been thought to play a role in charge neutralization.) Negative ions are confined to the bulk plasma and cannot reach the surfaces until the sheath voltage has completely collapsed, which is not expected to happen until ion-ion plasma is formed. During the after-glow period of electronegative plasma, the electron temperature is low and so the plasma potential is also low. The time scale for the transition to ion-ion plasma is typically many tens of microseconds and is strongly dependent on the gas mixture, pressure, and RF power. For example, although Cl_2 is a thermally attaching molecule, high RF power would increase the dissociation fraction of Cl_2. This, in turn, would lower the rate of dissociative attachment; the potential shortage of Cl_2 molecules could prevent ion-ion plasma from forming or delay its formation until very late in the after-glow. However, depending on the reactor wall coating, this effect may be negated by plasma-surface interactions that lead to changes in Cl_2 densities.[64,65] Similarly, if the feedstock gas is diluted in Ar, the negative ion density is typically too low to enable transition to ion-ion plasma. Subramonium and Kushner[44] found that for their discharge configuration, at a pulse frequency of 10 kHz and 50% duty cycle, the Cl_2 mole fraction should be greater than 50% for significant Cl^- extraction.

Using numerical modeling of typical time modulated high-density Cl_2 plasmas, Ashida and Lieberman[54] demonstrated that it is possible to extract negative ions at the walls only for after-glow periods of longer than several tens of microseconds. For their specific conditions, they showed that the Cl^- flux to the walls is dominant 35 μs *after* the source has been turned off. The Ashida–Lieberman model predicts that the time required for the negative ion flux to dominate increases when pressure is lowered (which decreases the rate of dissociative attachment in the after-glow) and/or when duty cycle increases. Malyshev *et al.*[49] investigated the time dependence of electron, positive, and negative ion densities, and electron temperature in a Cl_2 high-density, transformer-coupled pulsed plasma. They demonstrated that during the after-glow, electron density decreases rapidly, leading to Cl^- formation by dissociative attachment of Cl_2. Formation of Cl^- is

accelerated at higher Cl_2 densities, as may be the case, for example, at high pressures and low powers.

Malyshev *et al.*[49] demonstrated that ion-ion plasma forms toward the end of the after-glow (for an after-glow duration between 50 and 100 μs) when the sheath collapses and Cl^- ions can reach the wafer. This observation agrees well with the time scales predicted by the Ashida–Lieberman model. In contrast to Cl_2 plasmas, Overzet *et al.*[34] has shown that in highly attaching gas mixtures (e.g., SF_6), significant fluxes of F^- reach the surfaces very early into the after-glow period (about 10 μs). The shorter transit time stems from both the higher electronegativity and higher mobility of F^- compared to Cl^-.

3. Impact on IEDF

In the absence of a substrate bias, the ions arrive at the wafer with energies approaching the bulk plasma potential. In a pulsed operation, since the plasma potential attains a nominal value of 15–30 eV during the active-glow this also represents the energy of the ions. In the after-glow, the plasma potential decreases, leading to very low energy ions. For example, the variation in the time-averaged IEDF with duty cycle is shown in Fig. 7 in Ar microwave plasma for a peak power of 960 W, pulsed at 1 kHz.[66]

The multiple peaks of the IEDF reflect the contributions of ions arriving during the active-glow (populating the high-energy peak 1), those arriving during the after-glow (low-energy peak 2), and those arriving during the early active-glow as a consequence of T_e overshoot (highest energy peak 3). The relative ratio of peaks 1 and 2 is modulated by varying the duty cycle while the height of the highest energy peak (peak 3) increases slightly with pulsing frequency. Similar IEDF structures have been confirmed by different experimental studies utilizing different measurement methods (Conway *et al.*,[67] Zabeida *et al.*[68] with multigrid retarding field energy analyzer; Voronin *et al.*[69] and Wang *et al.*[70] with mass spectrometry). During the after-glow, low-energy ions may be easily deflected by negative charges accumulated on the resist mask sidewalls, helping to mitigate differential charging.[14]

B. Dynamics in the presence of substrate bias

Biasing of the substrate (i.e., capacitively coupling the power) is typically used to affect the shape of the energy distribution function of ions incident on the wafer. However, when pulsing a high-density plasma source, adding substrate bias increases the degrees of freedom by which the discharge characteristics can be modulated. For example, an appropriate choice of the bias frequency can allow for efficient extraction and subsequent acceleration of negative ions from the bulk to etch the wafer and/or facilitate neutralization of charge buildup on the wafer surface. Hence, the substrate bias can be used in conjunction with the pulsed plasma source in three different configurations, i.e., source pulsing (bias is in CW), bias pulsing (source is in CW), and synchronous or embedded pulsing (both source and bias are pulsed at the same frequency and at the same or different duty cycles, respectively).

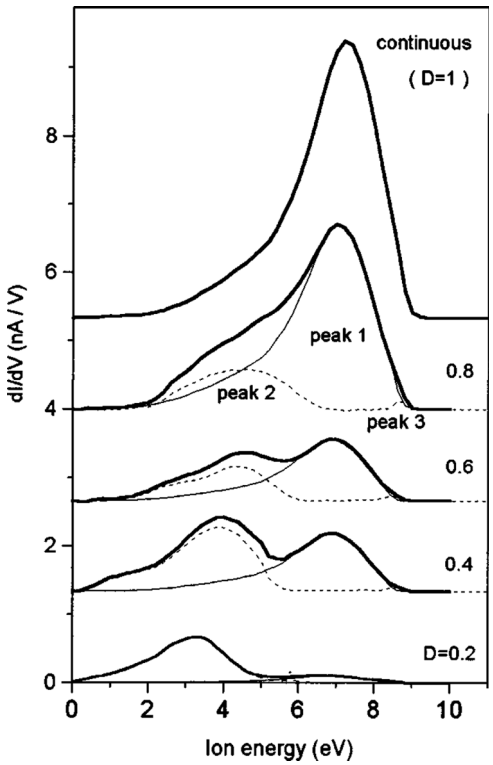

FIG. 7. Ion energy distribution functions in Ar microwave plasma with a peak power of 960 W pulsed at 1 kHz for varying duty cycles (D). Ion energies reflect the period of the pulse from which they originate depending on the duty cycle of the pulse. Reprinted with permission from O. Zabeida and L. Martinu, J. Appl. Phys. **85**, 6366 (1999). Copyright 1999, American Institute of Physics.

1. Continuous substrate bias

Malyshev and Donnelly[71] were the first to report on the capacitively coupled discharge that sustains during the late after-glow when an RF bias is applied continuously to the wafer in a pulsed Cl_2 ICP discharge. Subramonium and Kushner[58,72] computationally investigated the characteristics in the same chamber and found very good agreement with the observations of Malyshev and Donnelly,[71] as shown in Fig. 8. During the active-glow and initial after-glow, the temporal characteristics of n_e and T_e are, for the most part, invariant in the presence of the RF bias (compared to no bias). However, in the presence of RF bias, they observed an increase in T_e after $\sim$20 μs into the after-glow, attributed to the rapidly decaying electron density to the point when sheath heating exceeds the thermal and inelastic losses. Late in the after-glow period, n_e saturates to a low value when the capacitively coupled RF bias power sustains the discharge in a capacitive mode. The onset of the capacitive mode was shown to occur earlier in the after-glow with increasing RF bias amplitude.

An important conclusion noted by Malyshev and Donnelly[71] is that the presence of the continuous RF bias at high frequency prevents the sheath collapse that occurs in the absence bias and therefore bars negative ions from reaching the wafer. Although its impact on the ion energy distribution characteristics (broad energy range) make a low RF frequency

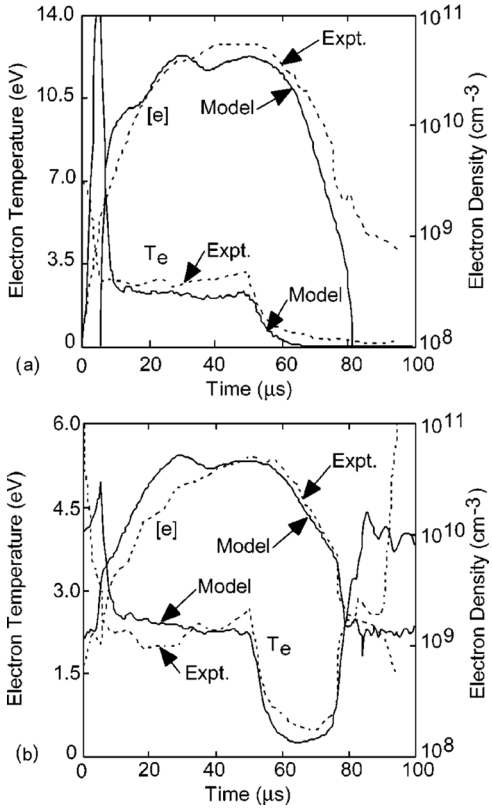

FIG. 8. Temporal dynamics of electron temperature and electron density in (a) absence of bias and (b) presence of bias in Cl_2 ICP plasma with a peak power of 600 W pulsed at 10 kHz and a duty cycle of 50%. Sheath heating during the late after-glow leads to a capacitive discharge with higher electron temperature. Reprinted with permission from P. Subramonium and M. J. Kushner, Appl. Phys. Lett. **79**, 2145 (2001). Copyright 2001, American Institute of Physics.

bias less desirable, it may facilitate negative ions to reach the wafer. For example, the effect of continuous RF bias at low frequency on the etch rate and etching characteristics was previously investigated by Samukawa.[30] Samukawa found that the polysilicon etch rate increased with greater pulse frequency in a Cl_2 microwave plasma pulsed with a duty cycle of 50% and utilizing a low RF bias frequency of 600 kHz. In contrast, the etch rate did not change when the bias frequency was increased to 2 MHz. This enhancement in etch rate is attributed to the acceleration of both positive and negative ions facilitated by the low RF frequency. The etch profile characteristics at 600 kHz also indicated less sidewall notching at the bottom of the feature—further evidence of negative ions making it to the bottom of the feature.

The transition to a capacitive discharge during the after-glow has important consequences on the characteristics of ion energies incident on the wafer. For example, the self-generated dc bias is strongly modulated when only the source power is pulsed.[73] In particular, the plasma density decay during the after-glow leads to lower ion fluxes (or current) to the wafer. As a result, higher voltages are required to deposit the desired bias power, leading to higher ion energies during the after-glow compared to the active-glow. For example, Agarwal *et al.*[73] computed the pulse-averaged IEDFs during the pulse as shown in Fig. 9(a) for an Ar/Cl_2 ICP plasma with a peak power of 300 W pulsed at 5 kHz with a 50% duty cycle. The peak bias power is 100 W. While the ion energies during the active-glow peak at around 100 eV, those during the after-glow are in the range of 250–350 eV.

The predicted ion energy characteristics agree qualitatively with the measurements of Zabeida *et al.*,[68] as shown in Fig. 9(b), who observed a similar shift in their pulsed microwave discharge with a continuous RF substrate bias. They observed ions with a much broader energy range and multiple IEDF peaks during the after-glow, attributing this to the modulation of the self-generated dc bias. These temporal changes in the self-generated dc bias were also reported by Agarwal *et al.*[73] It has been reported that the silicon etch rate during pulsing does not decrease commensurate with the duty cycle.[73] That is, for a duty cycle of 50% the etch rate does not decrease to 50% of that achieved in CW mode. The high ion energies during the after-glow are, in part, responsible for this sub-linear scaling of etch rate

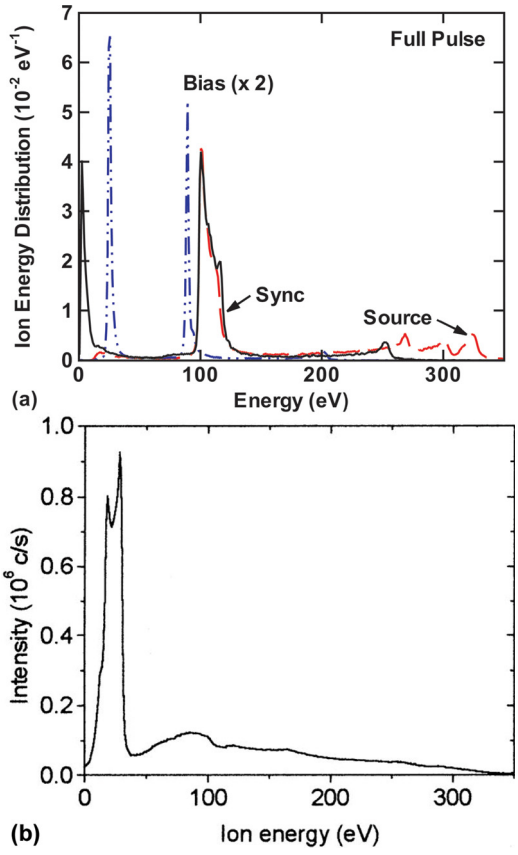

FIG. 9. (Color online) (a) Model predicted pulse-averaged ion energy distributions, labeled as Source, for a 10 mTorr Ar/Cl_2 ICP plasma with a peak ICP power of 300 W pulsed at 5 kHz and 50% duty cycle and 100 W bias power in continuous mode. Reprinted with permission from A. Agarwal, P. J. Stout, S. Banna, S. Rauf, and K. Collins, J. Vac. Sci. Technol. A **29**, 011017 (2011). Copyright 2011, American Vacuum Society. (b) Experimentally measured average ion energy distribution signal in 100 mTorr Ar microwave plasma with a peak microwave power of 300 W pulsed at 1 kHz and 50% duty cycle and continuous RF substrate bias. Reprinted with permission from O. Zabeida, A. Hallil, M. R. Wertheimer, and L. Martinu, J. Appl. Phys. **88**, 635 (2000). Copyright 2000, American Institute of Physics.

with the effect (high ion energies leading to etch enhancement) being stronger at lower duty cycles.

2. Pulsed substrate bias

Most plasmas used for materials processing utilize electronegative gas mixtures in which a significant number of electrons may be lost via dissociative attachment to form negative ions. The low mobility of negative ions ultimately minimizes their direct impact on surface reaction. As some experiments (in the absence of bias) indicated that the plasma transitions to an ion-ion plasma, there was renewed hope of utilizing the negative ions. However, as discussed above, with most industrial plasmas employing a substrate bias to enhance etch rates, a continuous substrate bias allows the plasma to transition to a capacitive mode that prevents the negative ions from reaching the wafer. Although the transition to capacitive discharge may be delayed by reducing the electronegativity of the feedstock gas[70] (e.g., diluting Cl_2 with Ar), this strategy adversely affects negative ion production, leading to a very low negative ion flux signal at the wafer. It then naturally follows that pulsing the substrate bias in addition to the ICP source may enable negative ions to reach the wafer in the after-glow. This also increases the degrees of freedom to use the discharge to modulate the plasma properties.

Kanakasabapathy *et al.*[35] experimentally demonstrated alternating fluxes of positive and negative ions incident on the wafer when the RF bias is applied exclusively in the after-glow of the ICP pulse. Once the plasma transitioned to an ion-ion plasma during the after-glow, a low frequency (20 kHz) bias was applied to enable extraction of the positive ions during the cathodic half of the RF cycle and negative ions during the anodic half (Fig. 10). Although negative ion extraction is facilitated by the low frequency bias (thereby increasing the time over which these ions are preferentially accelerated), the ions that arrive at the wafer do so only with thermal energies as the ion transit time through the sheath is much greater than the 20 kHz period of 50 μs, i.e., the time for negative ions to traverse the sheath is much greater than the period for which the RF is applied. Similarly, Walton *et al.*[74] also demonstrated alternating fluxes of positive (SF_5^+) and negative (SF_5^-) ions in Ar/SF_6 (50/50) plasma with a bias frequency of 10 kHz in pulsed electron beam plasmas.

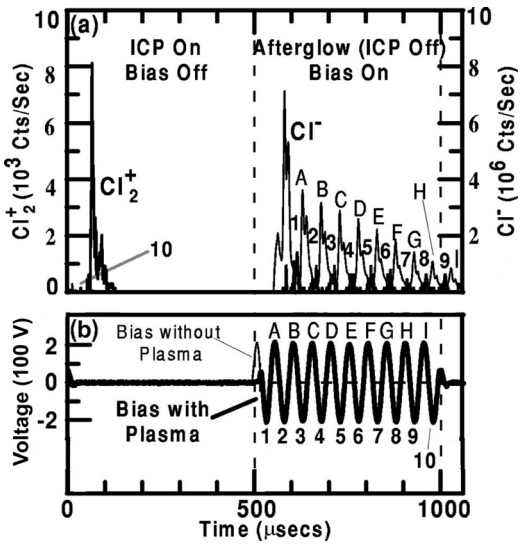

FIG. 10. Mass spectrometer signals for (a) Cl^+ and Cl^-, and (b) applied bias voltage measured in a 1 mTorr, 5 sccm Cl_2 ICP plasma with a peak ICP power of 600 W pulsed at 1 kHz and 50% duty cycle. The bias operates at an excitation frequency of 20 kHz with a peak voltage of 225 V. Reprinted with permission from S. K. Kanakasabapathy, L. J. Overzet, V. Midha, and D. Economou, Appl. Phys. Lett. **78**, 22 (2001). Copyright 2001, American Institute of Physics.

Most industrial plasmas do not use RF bias at such low frequencies due to the significant impact on the shape of the IEDF of the positive ions impinging on the wafer (in particular during the CW process). RF bias at low frequencies not only leads to higher ion energies at the wafer, but also significantly increases the energy spread of the ions, which ultimately has implications for tuning ion energies to achieve the desired precision (e.g., etch selectivity). To that end, Subramonium and Kushner[72] explored alternatives for accelerating negative ions toward the wafer while using reasonably high RF bias frequencies in the megahertz range. They concluded that by pulsing the RF bias out of phase with the ICP pulse, negative ion extraction is possible even for a bias frequency of 10 MHz as the transition to a capacitive heating mode is delayed. However, because of the earlier onset of the capacitive heating mode, negative ion flux so extracted will decrease as voltage amplitude increases. Further, with a 10 MHz bias frequency, the ions thus extracted in the after-glow have only thermal energy as the applied RF voltage is dominantly dropped across the bulk plasma. As the bias frequency decreases, sheath formation increases the energy of negative ions incident on the wafer. For example, negative ions are extracted with an average energy of 9 eV at RF bias frequency of 2 MHz. Although extraction of negative ions has been conclusively demonstrated in pulsed plasmas, the strategies employed may not necessarily have a broad enough operating window to be of much consequence. Further, as plasma density is typically low in the after-glow, the flux of the negative ions thus extracted is at least an order of magnitude lower than the flux of positive ions during the active-glow.

Measurement complexity accounts for a notable scarcity of experimental data in the literature addressing the impact of a pulsed substrate bias on ion energy characteristics. Banna *et al.*[22] and Agarwal *et al.*[23] have computationally investigated the impact of a pulsed substrate bias on ion energy. In particular, IEDFs were characterized independently over the pulse period by subdividing the active-glow into three segments and the after-glow into two. The IEADs over the bias (at 13.56 MHz) pulse are shown in Fig. 11(a) for an Ar/Cl_2 plasma pulsed at 5 kHz with a 50% duty cycle. Note that the RF bias is pulsed in-phase with the ICP source pulse. The ramp-up (-down) phase refers to when the RF bias power increases (decreases) to its peak value (zero) while the top-flat phase refers to when the peak power is deposited.

The distribution functions indicate a nominal peak around 100 eV with a long high-energy tail (up to 250 eV). The

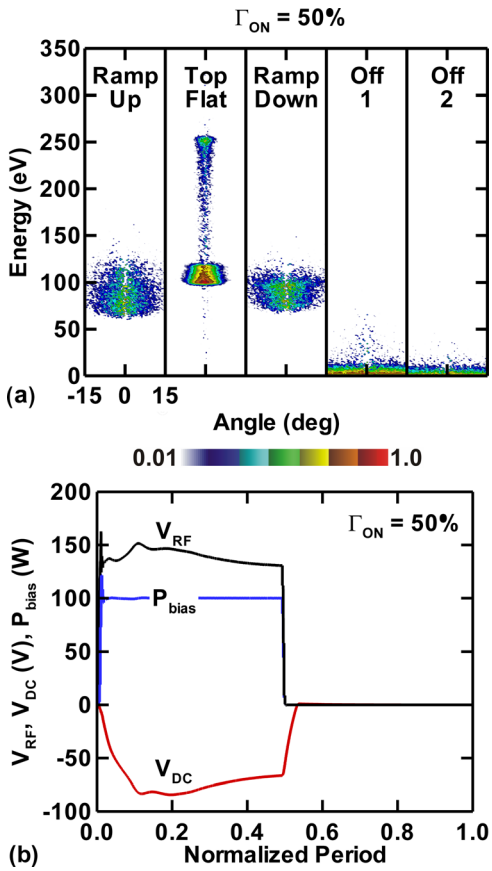

FIG. 11. (Color online) (a) Ion energy and angular distribution functions and (b) RF bias voltage, self-generated dc bias during the pulse in Ar/Cl_2 (10 mTorr, 100 sccm) plasma when the ICP source (peak power 300 W) and bias (peak power 100 W) are pulsed in phase at 5 kHz and 50% duty cycle. The overshoot in the supply voltage leads to a high energy tail in the top-flat phase of the pulse. Reprinted with permission from A. Agarwal, P. J. Stout, S. Banna, S. Rauf, K. Tokashiki, J.-Y. Lee, and K. Collins, J. Appl. Phys. **106**, 103305 (2009). Copyright 2009, American Institute of Physics.

high-energy tail observed is greater than the self-generated dc bias that develops and owes its origin to the overshoot of the RF bias voltage at the beginning of the pulse, as shown in Fig. 11(b). This overshoot results from the low initial density, leading to lower ion currents. As the ion density increases during the active-glow, the RF bias voltage reaches a quasi-steady state, leading to peak energy near 100 eV. The ion energies are in the range of 65–100 eV during the ramp portions of the pulse. They are, on average, higher during the ramp-down portion of the pulse due to the self-generated dc bias on the blocking capacitor, which discharges on a time scale longer than the ramp-down time. In the after-glow, ion energies subsequently drop to a very low value owing to decay of the bulk plasma potential and discharging of the blocking capacitor. As both the ICP and bias powers are pulsed, the phase difference between the pulses can additionally be varied to further tailor ion energy and angular distribution characteristics.

Variations in IEAD characteristics result from varying levels of ion densities and fluxes to the wafer, which govern the RF bias voltage required to achieve a desired bias power deposition. Agarwal *et al.*[23] have also investigated the impact of varying phase between the ICP and bias pulses on ion energy characteristics among others. Their conclusions are easily understood based on the earlier discussion of pulsing the bias and source completely out of phase to facilitate negative ion extraction. Plasma density decay during the after-glow necessitates a high supply voltage to achieve the desired bias power. Consequently, the self-generated dc bias voltage also increases (in magnitude) due to the low ion current; thus leading to higher ion energies. Higher ion currents cause the self-generated dc bias voltage to decrease during the active-glow of the source (ICP) pulse. Their predictions are in excellent agreement with the results of Shin *et al.*[75] who reported time-resolved RF voltage measurements on the RF biased electrode in a pulsed ICP plasma sustained in a fluorocarbon gas mixture. Ultimately, varying the phase between the source and bias pulses affords not only the possibility of extracting negative ions but also of tuning the IEDFs (especially increasing the ion energies), which is usually difficult to achieve in a CW plasma owing to the inherently higher ion currents of these plasma sources.

A subtle but important implication of the high-energy tail in the distribution functions at the leading edge of the bias pulse is the risk of ion-induced damage these energies pose for some critical applications. The scaling in ion energy at the leading edge can be significantly higher for plasmas sustained in more electronegative gas mixtures. Although the ion flux at these energies is typically low, the higher ion energies (than intended for the particular process) may adversely affect the damage precision requirements at advanced technology nodes. Therefore, Agarwal *et al.*[41] proposed an alternate pulsing scheme, wherein the inductive power is pulsed at a duty cycle larger than that of the bias power. They show that by increasing the phase lag between the bias and source power pulses, the high-energy peak during the leading edge of the bias pulse shifts toward lower energies. Such a scheme was found to have a marginal impact on etch depth while decreasing the possibility of ion-bombardment damage. It is worth noting that the impact of the high-energy tail can also be mitigated by varying the pulse ramp-up rate, and by varying the pulse frequency and duty cycle.[23]

To summarize, pulsing of the source strongly influences the bulk plasma characteristics (densities and electron temperature) while pulsing of the bias strongly modulates the characteristics of the IEADs. Pulsing of source and/or bias allows one to better tailor the energy characteristics of the ions incident on the wafer than when operating the bias in continuous mode.[23,41,73,76] The computationally predicted IEADs for various pulsing modes and the CW mode are shown in Fig. 12. The IEADs correspond to Ar/Cl_2 plasma sustained at 10 mTorr with 300 W ICP and 100 W bias. Either power source is pulsed, if at all, with a frequency of 5 kHz and a duty cycle of 50%, except for embedded pulsing mode in which the source is pulsed at 75% duty cycle. Note that the IEADs are referenced to the bias pulse. In all cases, the IEADs during the top-flat phase of the pulse closely resemble that achieved during the continuous mode except

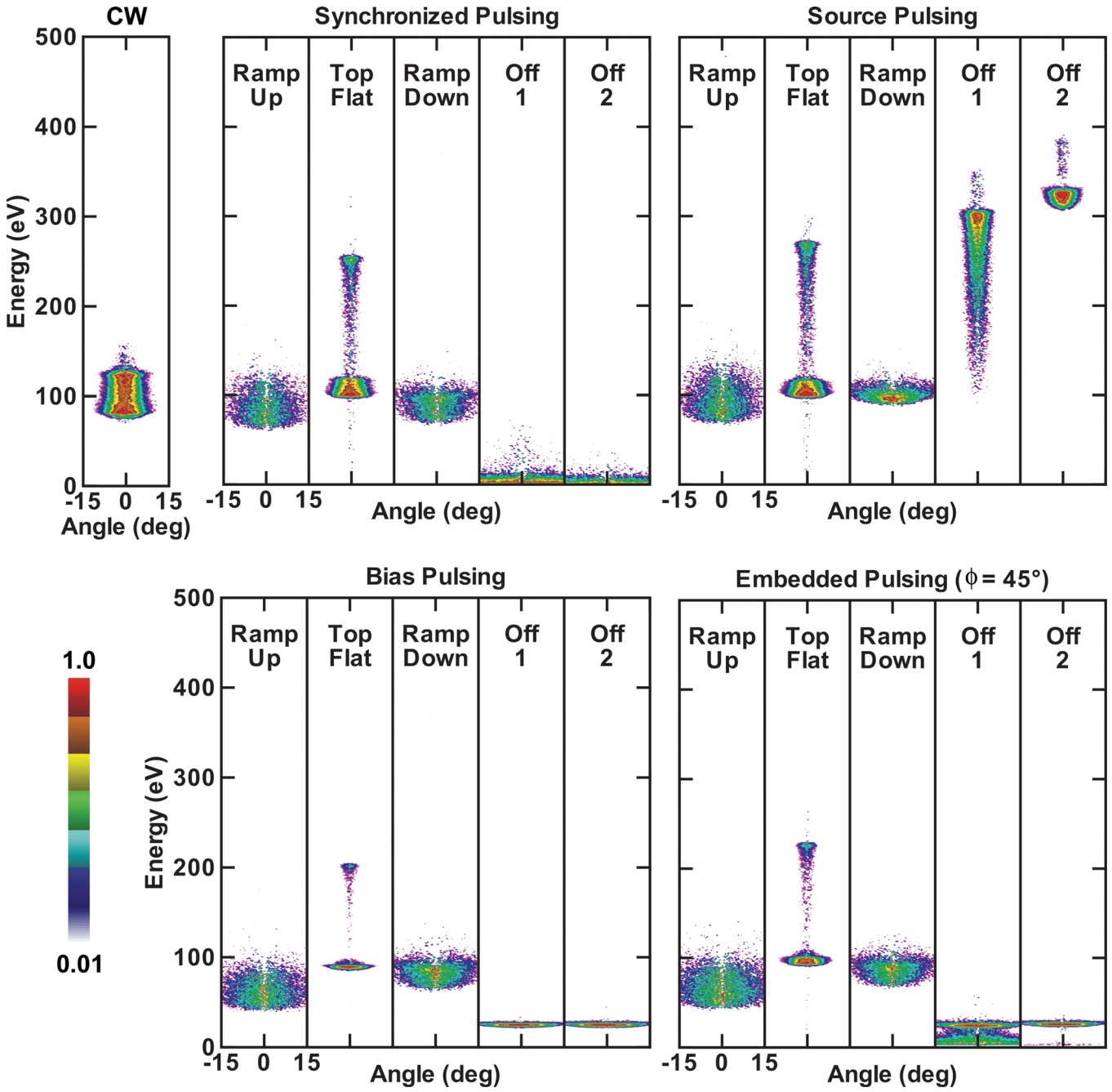

FIG. 12. (Color online) Comparison of ion energy and angular distributions during various pulsing modes and the continuous mode for an Ar/Cl_2 (10 mTorr, 100 sccm) plasma sustained in an ICP (300 W peak power) and a peak bias power of 100 W (Refs. 23, 41, 73). The pulse parameters are 5 kHz and 50% duty cycle. Synchronized pulsing refers to when sources are pulsed together (no phase lag); source pulsing refers to when only the source is pulsed with the bias in continuous mode; bias pulsing refers to when only the bias is pulsed with the source in continuous mode; embedded pulsing refers to when the source and bias are pulsed together with the bias pulse offset from the source pulse by the indicated ϕ. Reprinted with permission from A. Agarwal, P. J. Stout, S. Banna, S. Rauf, K. Tokashiki, J.-Y. Lee, and K. Collins, J. Appl. Phys. **106**, 103305 (2009). Copyright 2009, American Institute of Physics.

for the high-energy tail (intrinsic due to the initially low plasma density). The IEADs are strongly modulated during the after-glow as determined by the state of the source (active or not). While ion energies are very low (with wide angular distribution) during the after-glow phase of synchronized pulsing (due to the absence of power deposition), they are very high (with narrow angular distributions) during the after-glow phase of source pulsing as a result of the continuous bias (necessitating higher voltages due to the decaying plasma density). In contrast, ions arrive with moderate energies (commensurate with the plasma potential) during the after-glow when only the bias is pulsed. The angular width is broad as a result of the low sheath thickness.

Embedded pulsing mode embodies many synchronized pulsing characteristics except that the high-energy tail during the top-flat phase peaks to a lower energy (220 eV versus 260 eV). As the source is in effect for a larger fraction of the duty cycle, the IEADs during the after-glow vary. In particular,

the IEAD during the early after-glow phase (off-1) represents a combination of the IEAD in source pulsing and bias pulsing as ions arrive with the bulk plasma potential at the beginning of the off-1 phase and with only thermal energy toward the end of the off-1 phase. During the late after-glow phase (off-2), ions arrive with energies nominally equivalent to the plasma potential since source power has been turned on. One common characteristic of the IEAD during the after-glow is the wide angular distribution (except for source pulsing). This is of particular importance in achieving efficient reduction of charge buildup on the sidewalls of the feature being etched. In particular, synchronous pulsing is the only mode that creates wide angular distribution with extremely low energies ($\sim$1 eV) during the deep after-glow phase. Depending on the demands of the etch process, different pulsing modes allow one to tune the IEAD to achieve the desired etch profile.

C. Dynamics of radicals

The modulation of source power has a significant impact on radical composition in the bulk plasma due to a combination of at least two factors. As discussed in Sec. II B, modulation of source power leads to a lower electron temperature in the after-glow. As a result, the electron energy distribution function is populated with fewer (to no) electrons at energies sufficiently high to initiate dissociation of the feedstock gas in the after-glow, which leads to pronounced changes in the densities of radicals in the bulk plasma compared to CW plasma. In addition, the lack of continuous power deposition also alters gas-phase heating mechanisms, leading to modulation in gas temperatures as well,[77] which ultimately modifies not only the rate of heavy particle reactions in the gas phase but also affects the flux of the radicals to the wafer.

The impact of pulsing on radical densities is, however, complicated to characterize either experimentally or computationally. Although computational models of various complexities have been used to investigate the dynamics of charged species, little has been reported on the dynamics of radicals. This is due, in part, to the inherently transient nature of the model required to investigate pulsed plasmas. Further, the kinetics of neutral radicals evolve over a time scale that is much longer than the pulse period (as discussed below), requiring a prohibitively large number of pulse periods to be simulated to accurately capture the evolution of the radicals. Consequently, a prolonged execution time may be necessary for the model to ensure convergence on a pulse-averaged basis. To that end, volume-averaged global models are well-suited to provide some insight on the modulation of radicals in pulsed plasmas, although the impact on spatial distribution is still not known.

The challenges associated with experimental characterization are different. For example, detection of Cl and Cl_2 radicals in a Cl_2 discharge is often difficult.[78,79] High dissociation fractions in Cl_2 plasmas and weak absorption continuum makes it difficult to measure the absolute Cl_2 densities.[78] Similarly, calibration difficulties associated with laser-induced fluorescence (LIF) measurements can induce large errors in atomic Cl measurements.[79] Hence the reporting on experimental characterization of radical densities during pulsing in the literature is scarce. Similarly, probe measurements in certain gas chemistries (e.g., HBr/O_2 plasmas used for the over-etch process in gate etching) can be challenging given the rapid deterioration of the probe tip in the HBr environment. Bodart *et al.*[80] recently characterized radical densities in HBr pulsed plasmas using broadband UV and VUV absorption spectroscopy and modulated-beam mass spectrometry.

Experimental literature is, however, available for discharges sustained in fluorocarbon gas mixtures.[17,27,48,81–84] Pulsed plasma was used primarily to enhance the selectivity of SiO_2 etching to that of Si. In fluorocarbon etching of SiO_2, CF_2 radicals are involved in polymer generation that facilitates the SiO_2 etching while preventing Si etching. On the other hand, F atoms are detrimental to selectivity as they spontaneously etch the underlying Si. Therefore, to improve selectivity in fluorocarbon plasma, it is important to achieve a higher ratio of CF_2 radicals to F atoms. Samukawa and coworkers[17,27,81] used actinometry to characterize F atoms and CF_2 radical generation in an ECR pulsed CHF_3 discharge and found that the ratio of F atoms to CF_2 radicals was low when the duty cycle of the pulse was low. This is attributed to the lower average electron temperature, which facilitates the low-energy dissociation process that generates CF_2 radicals over the high-energy dissociation processes that generate F atoms. Consequently, a highly selective process was achieved at lower duty cycles. This behavior was also confirmed in other fluorocarbon chemistries, such as C_2F_6 and C_3F_8,[81] and gas mixtures containing CF_4 (in particular H_2, via mass spectrometry by Sugai *et al.*[48])

Takahashi *et al.*[82] also investigated pulse modulated ECR plasmas using CHF_3 over a wide range of pulse frequencies (10–100 kHz). They characterized the modulation of CF_x ($x = 1 - 3$) densities using infrared diode laser absorption spectroscopy and also concluded that the ratio of CF_2 to F largely depended on the duty cycle. Hayashi *et al.*[83] used LIF to detect CF and CF_2 radicals in CF_4 (also CHF_3 and C_4F_8) ICP discharge over a wide range of pulse frequencies (10–100 kHz). They found that while the ratio of CF_2 to CF radical densities modulated strongly with duty cycle, the ratio did not significantly change with the pulse frequency. Ultimately, though, the impact of the ratio of CF_2 to CF radicals has only a negligible effect on the selectivity of SiO_2 to Si. Similarly, Yamanaka *et al.*[84] later characterized (using LIF) a pulsed ICP discharge sustained in CHF_3/C_4F_8 (50/50) mixture and arrived at the same conclusions as Hayashi *et al.*[83] All these studies converge toward the same conclusion: plasma chemistry can be controlled by the duty-cycle.

While similar characterization in Cl_2 plasmas has not been done (halogen-based chemistries are most often used for etching of polysilicon stacks), global models[46,54–56] enable characterization of the radical density variations in pulsed Cl_2 plasmas. Consider, for example, a Cl_2 plasma discharge at 10 mTorr in a high-density source chamber to etch wafers with 300 mm diameter. The typical volume of such a design is about 30–40 l. In the active-glow, Cl atom production is

governed by the electron impact dissociation of the Cl_2 feedstock molecules. The build-up rate of the radicals is then given by $\nu_{rise} = k_{diss} n_e$, where k_{diss} is the dissociation rate. For a nominal $k_{diss} = 10^{-8}\,cm^{-3}\,s^{-1}$ for Cl_2 molecules, the typical rise time is then given by $1/\nu_{rise} = 10^{-3}$ s. As the electron temperature drops rapidly ($\sim 10\,\mu s$) during the afterglow, electron energy is, for the most part, below the dissociation threshold. The kinetics of the radicals is thus governed only by loss mechanisms due to sticking or recombination on the reactor walls and via pumping, the typical rate of which is less than $50\,s^{-1}$. The loss rate of radicals on the walls of the reactor is dependent on its diffusion coefficient (a function of pressure and temperature) and the sticking coefficient (a function of both radical and surface identities).

Calculations based on the diffusion equation show that the total decay rate, ν_{decay}, is on the order of $100\,s^{-1}$ and generally does not exceed $1000\,s^{-1}$. The as-predicted decay rates are in good agreement with experimentally reported decay rates for gas mixtures such as fluorocarbon, Cl_2 and N_2/H_2. Simple estimations of the build-up and decay rates agree well with the values used by Lieberman and Ashida,[46] who used values of 2600 and $600\,s^{-1}$ for ν_{rise} and ν_{decay}, respectively.[85–92]

Note that for a typical pulsing frequency of 10 kHz, the pulse period is only $100\,\mu s$, but is sufficiently long to induce significant temporal variations in the charged species (electrons and ions) and electron temperature (which vary on time scales of $10\,\mu s$). In contrast, the pulse period time scale to induce any significant variation in the density of radicals during the pulse is many orders of magnitude smaller. Thus, for the most part, the density of radicals is invariant during the pulse and a time-averaged value, $\langle n \rangle_t$, is sufficient to understand the dynamics of pulse parameters of interest. For example, the time-averaged value of the ratio of atomic to molecular chlorine in a pulsed discharge is given by[46]

$$\frac{\langle Cl \rangle}{\langle Cl_2 \rangle} = \frac{2\langle k_{diss} n_e \rangle}{\nu_{decay}}. \tag{5}$$

Therefore, for a given duty cycle the time-averaged value of the dissociation rate is invariant with the frequency of the pulse.[46,54] Accordingly, pulse frequency is not expected to strongly modulate the atomic radical density and hence does not have a significant impact on the plasma chemistry as long as the pulse period is shorter than the rise/decay time of radicals (i.e., $\sim$1 ms). However, as the dissociation rate is a function of electron temperature, which is strongly modulated between the active- and after-glow phases of a pulse, the duty cycle of the pulse does significantly affect the dissociation rate and hence the production of atomic radicals. As the residence time of the feedstock molecules is long (100 ms) compared to the pulse period, the total amount of time during which feedstock molecules interact with high-energy electrons to initiate dissociation processes determines the atomic radical densities. This explains the strong dependency of radical densities on duty cycle but not on pulsing frequency.

This observation was recently experimentally characterized by Bodart *et al.*,[80,93] who demonstrated modulation of the ratio of Cl to Cl_2 densities with duty cycle while the ratio was found to be independent of the pulse frequency. The experimentally measured Cl_2 and Cl densities in Cl_2 plasmas are shown in Figs. 13(a) and 13(b) for varying duty cycles. The pulse frequency is 1 kHz for Cl_2 density measurement while Cl density was measured at a pulse frequency of 5 kHz. The density of Cl_2 decreases as duty cycle increases, leading to increased production of Cl radicals. Although not exactly at steady state, Agarwal *et al.*[23] observed, in their computational investigation of pulsed plasmas, similar trends in Ar/Cl_2 plasma, as shown in Figs. 13(c) and 13(d). The lower Cl radical density during pulsing ultimately affects the ion-to-neutral flux ratio incident on the wafer, which, in turn, affects the evolution of etch. The dependence of radical densities on the pulse duty cycle and invariance with pulse frequency also explains the results of Haass *et al.*,[94] who found that the Si etch rate in pulsed HBr/O_2 plasmas was invariant with the pulsing frequency (in the range of 0.5–1 kHz) but strongly dependent on the duty cycle.

Although the analysis above assumed no interaction between gas phase radicals and etch by-products, the conclusions can be carefully extended to conditions for which the assumption may not be valid. For example, the density of etch by-products, such as $SiCl_x$ radicals or BCl (in BCl_3 plasmas as might be used for etching of Hf-based dielectrics) may also be modulated during pulsed operation. The kinetics of heavy-particle bimolecular reaction of the type $SiCl + Cl_2$ yielding $SiCl_2 + Cl$ will ultimately be affected by the higher density of feedstock molecules at lower duty cycles. This was experimentally observed by Vempaire and Cunge,[95] who showed that such reactions could proceed at very high rates (up to $10^4\,s^{-1}$), leading to significant changes in the chemical composition of the plasma. In fact, they observed that the radical density is not independent of the pulse frequency. Ultimately, the analysis of radical interactions is complex and their density dependence on pulse parameters of interest difficult to assess due to their long time scale of evolution. This is an area of potential opportunity in pulsed plasmas. A significant number of experimental studies are necessary to accurately characterize the dynamics of radicals in pulsed plasmas.

III. EARLY USE OF PULSED PLASMAS IN ETCH APPLICATIONS

Since the late 1980 s, pulsed plasmas have been investigated by research groups at universities and laboratories worldwide for etching a wide range of materials used in microelectronics. In this section we review the major benefits of pulsed plasmas over conventional CW plasmas for conductor (including magnetic) materials and dielectrics as reported over the past three decades.

A. Pulsed plasmas for conductor etching

In one of the early papers on etching with pulsed plasmas, Boswell and Porteous[96] investigated etching of silicon in pulsed SF_6 plasmas. They demonstrated that for short pulses

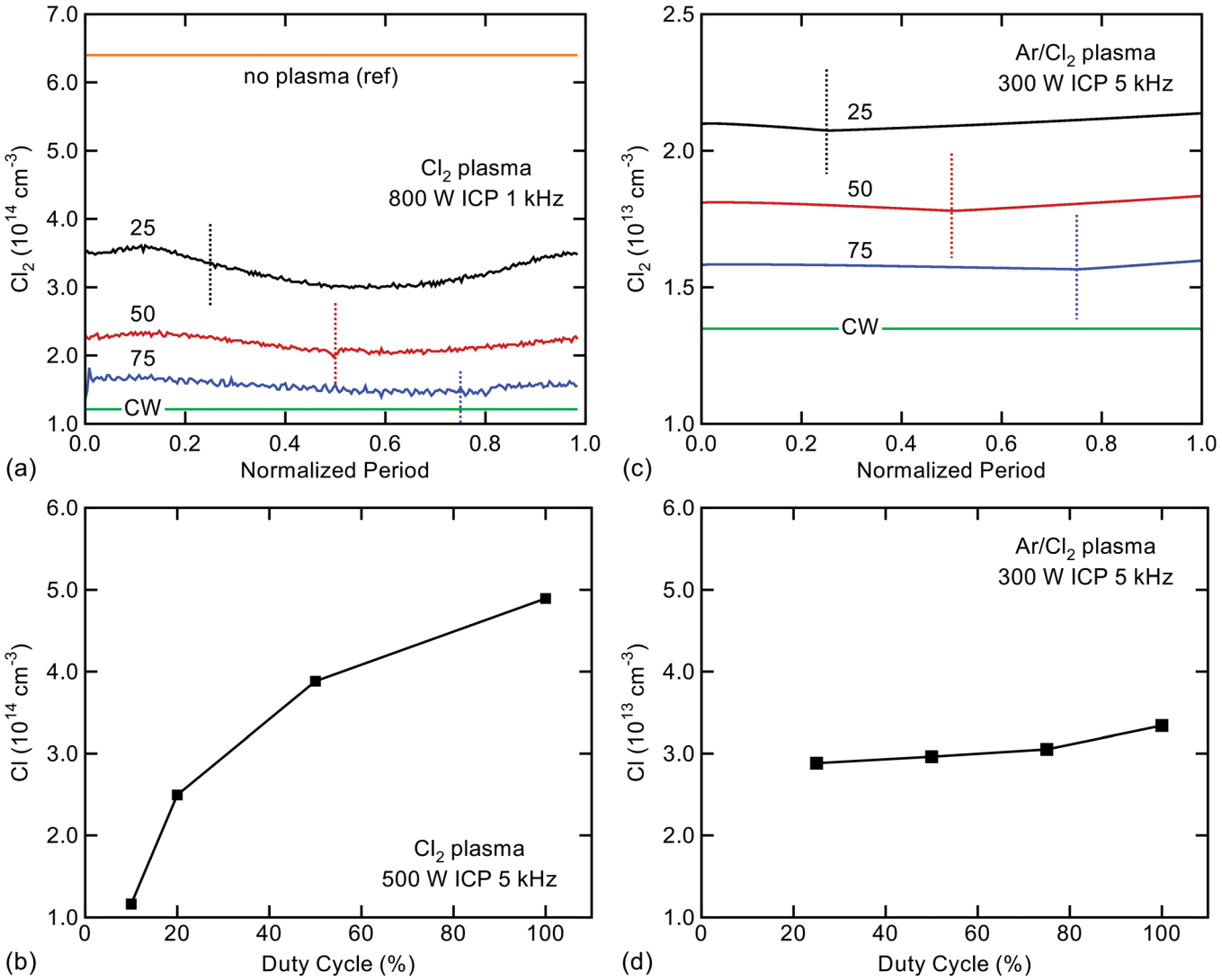

FIG. 13. (Color online) Gas dissociation decreases during pulsed plasma operation leading to lower reactive radical densities. Experimentally measured (a) temporal dynamics of Cl_2 density (Cl_2, 800 W ICP pulsed at 1 kHz) and (b) pulse-averaged Cl density (Cl_2, 500 W ICP pulsed at 5 kHz) as a function of duty cycle (Refs. 80 and 93). Model predicted (c) temporal dynamics of Cl_2 density (Ar/Cl_2, 300 W ICP pulsed at 5 kHz) and (d) pulse-averaged Cl density (Ar/Cl_2, 300 W ICP pulsed at 5 kHz) as a function of duty cycle. The computationally predicted trends are in good agreement with the experimental observations. Reprinted with permission from P. Bodart, M. Brihoum, G. Cunge, O. Joubert, and N. Sadeghi, J. Appl. Phys. **110**, 113302 (2011). Copyright 2011, American Institute of Physics.

(pulse frequency >100 Hz), the silicon etch rate in a pulsed plasma was essentially the same as for continuous plasmas, despite a low duty cycle of 20%. From these experiments, they concluded that fluorine atoms created by the plasma during the active-glow period are long-lived and etch silicon during the after-glow of the pulsed discharge.

Similarly, Petri *et al.*[97] investigated pulsed plasma strategies with the objective of understanding tungsten etch mechanisms using SF_6. They found that the etch rate of tungsten in pulsed SF_6 discharges was higher than in CW discharges, while the experimental results also demonstrated that fluorine adsorption on the tungsten surface continued to saturation in the after-glow. From the etch rate measurements, as a function of duty cycle, Petri *et al.*,[97] concluded that tungsten etching is fluorine adsorption limited for larger duty cycles and etch product desorption limited for smaller duty cycles.

In the mid-1990 s, numerous studies addressed gate etching processes in Cl_2-based plasmas. Multiple teams were involved in this work with emphasis on fundamental understanding of pulsed chlorine plasmas. Samukawa and his team extensively investigated polycrystalline silicon etching using pulsed Cl_2 ECR plasma.[15,29] In their study, the pulse duty cycle was maintained at 50% while the active-glow time was varied from 10 to 100 μs. They reported that the average etch rate of polycrystalline silicon for low pulse frequencies (<10 kHz) was similar to that in CW plasmas. Pulsing conditions could be found for which the polysilicon etch rate was close to the etch rate obtained in CW discharges while the SiO_2 etch rate decreased significantly [Fig. 14(a)]. They explain that, in the after-glow, the oxide etch rate—which is more ion-assisted than in polysilicon etching—decreases sharply as ion energies decrease, while polysilicon etching continues, in effect leading to an increase

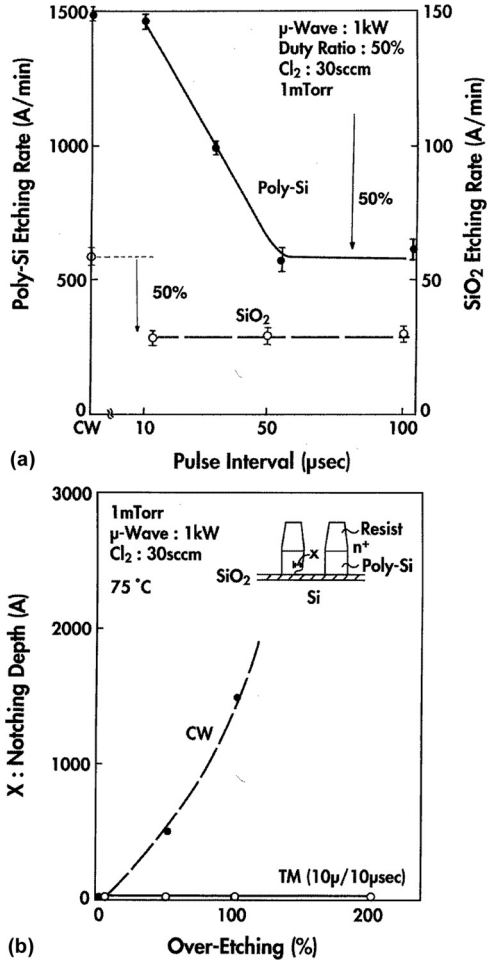

FIG. 14. (a) Etch rates of poly-Si and SiO_2 in Cl_2 (30 sccm, 1 mTorr, 1 kW) microwave plasma as a function of the pulse duration for a constant 50% duty cycle. (b) Notch depth at the foot of phosphorus-doped poly-Si as a function of over-etching time under CW and pulsed (50 kHz, 50% duty cycle) conditions in Cl_2 (30 sccm, 1 mTorr, 1 kW) microwave plasma. Reprinted with permission from S. Samukawa and T. Mieno, Plasma Sources Sci. Technol. **5**, 132 (1996).

in the selectivity between polysilicon and SiO_2. Although severe notching was observed in the CW Cl_2 plasma, pulsed Cl_2 ECR plasmas could fully eliminate the notch even at 200% over-etch time [Fig. 14(b)]. Based on these results, they concluded that time modulated plasma reduces the amount of charging on the surface of SiO_2, but offered no detailed explanations. The role of negative ions was also suspected by Samukawa and his team based on a preliminary study by Overzet *et al.*[98]

The decrease in notching when using pulsed plasmas has often been attributed to negative ions. If true, the time required for the sheath voltage to collapse is the critical parameter for negative ions to neutralize surface charge. Unless special techniques are utilized, negative ions reach the wafer only after a long period of time in the after-glow of Cl_2 plasmas, as discussed earlier. Further, enhancement of the etch rate is possible only if the negative ions are accelerated enough, which can be done by using a very low frequency bias power supply. Therefore, negative ions are not expected to be useful when the plasma is pulsed at frequencies higher than 5 kHz (assuming a nominal duty cycle of 50% and a nominal after-glow period of at least 50 μs for negative ion extraction) and their role in charge reduction may have been overestimated in the literature. For example, Ahn *et al.*[20] investigated mechanisms of silicon gate etching in pulsed Cl_2 plasmas by measuring such key parameters as negative ion (Cl^-) density, electron density, electron temperature, and plasma potential. In particular, absolute Cl^- measurements, combining photo-detachment and plasma oscillations methods, indicated that significant concentration of negative ions were generated at the beginning of the after-glow that decays in the late after-glow [Fig. 15(a)].

Contrary to the assumptions of Samukawa *et al.*,[15,29] Ahn *et al.*[20] found negative ions to be confined by a positive space-charge sheath until the late after-glow and hence, are unable to contribute to surface charge neutralization. Similar to Samukawa, Ahn *et al.*[20] demonstrated that notching could be eliminated when the Cl_2 ECR plasma operates in the

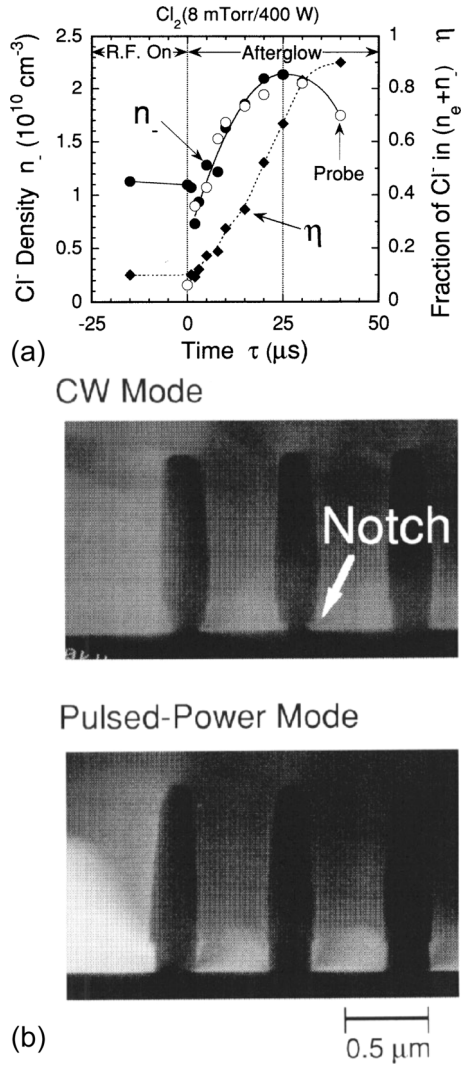

FIG. 15. Plasma and etch properties in Cl_2 (8 mTorr, 800 W) ICP pulsed at 10 kHz and 50% duty cycle. (a) Temporal dynamics of Cl^- density (left axis) measured by the plasma oscillation method (closed circles) and by the probe method (open circles) and negative ion fraction (right axis, diamond) and (b) cross sectional SEM of the gate poly-Si profile etched in CW and pulsed modes. Reprinted with permission from T. H. Ahn, K. Nakamura, and H. Sugai, Plasma Sources Sci. Technol. **5**, 139 (1996).

pulsed mode while a low voltage CW RF bias is applied to the wafer [Fig. 15(b)]. They suggested that the positive charge built up on the gate oxide surface could be neutralized during the after-glow by high electron flux with a narrow beam velocity distribution. However, this is quite unlikely as, in the presence of a normal positive space charge sheath, electrons will likely not be accelerated to form a directional beam. In another experiment, a positive square wave pulse was applied to the substrate in the after-glow of the ECR source, with the objective of using negative ions for polysilicon etching. Based on the etch rate measurements, Ahn *et al.*[20] concluded that negative ions can assist etch reactions as do positive ions. In this experiment, the RF bias frequency was lowered from 13.56 MHz to 600 kHz. Etch rates obtained at 600 kHz are higher than at 13.56 MHz as a large contribution to etch reactions is now expected from the negative ions. Ahn *et al.*[20] concluded that, in low bias frequency conditions, both positive ions created during the active-glow of the plasma and negative ions generated during the after-glow are involved in the etching process.

An alternative mechanism for charge reduction was given by Hwang and Giapis,[14] who proposed that positive ions with low-energies, as a consequence of lower electron temperature during the after-glow, are responsible for reducing the charging potential at the trench bottom surface. The low-energy positive ions, deflected by smaller local electric fields during the after-glow, reach the upper mask sidewalls (where electrons accumulate), thereby lowering the negative entrance potential for electrons. As a result, electrons reach the bottom of the feature and neutralize the positive charge accumulated there. While this suggested mechanism applies early in the after-glow, before the positive space charge sheath collapses, negative ions that exit the plasma later in the after-glow also help reduce the charge. Current balance of positive and negative charges is, therefore, accomplished at lower charging potentials along the patterned surface. As a consequence, distortion of ion trajectories is minimized and notch depth can be significantly reduced, if not eliminated.

This hypothesis was also supported by Maruyama *et al.*,[99] in their study of the impact of varying pulsing modes on selectivity of polysilicon to SiO_2 and notch depth in Cl_2/O_2 ECR plasma. They found that notch depth increased with aspect ratio when the ECR was operated in CW mode irrespective of the bias condition (with, without, and pulsed), as shown in Fig. 16(a). These findings indicate that the bias does not reduce charge build-up on the gate oxide. However, pulsing the ECR plasma source in the absence of bias noticeably decreased the notch depth compared to CW operation. As shown in Fig. 16(b), the dependence of notch depth on the features' aspect ratio also decreased considerably. In fact, for their operating conditions, they found synchronous pulsing to be the best way to minimize notch depth, suggesting that minimal charge build-up occurred in this mode. Notch depth reduction in pulsed ECR discharges compared to CW discharge when no bias was applied to the wafer was explained by low-energy electrons and an increase in the number of ions during the after-glow, which neutralized the charge build-up. The authors concluded that charge build-up

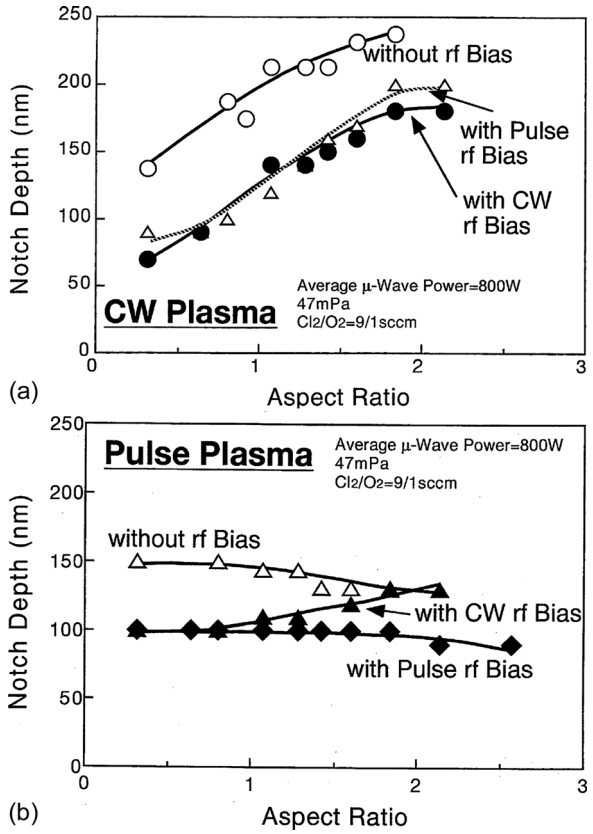

FIG. 16. Notch depth as a function of aspect ratio in $Cl_2/O_2 = 90/10$ (10 sccm, 3.525 mTorr, 800 W) ECR plasma. (a) CW plasma and (b) pulsed plasma conditions in the absence of, and the presence of, a continuous and pulsed RF bias on the wafer. Reprinted with permission from T. Maruyama, N. Fujiwara, S. Ogino, and H. Miyatake, Jpn. J. Appl. Phys. **37**, 2306 (1998). Copyright 1998, The Japan Society of Applied Physics.

reduction was greatest when both the bias and source powers are pulsed.

All the studies on notch evolution reviewed previously emphasize the electrical behavior of the discharge and the role of low-energy positive ions and negative ions formed during the after-glow. No information is given about the plasma chemistry and role of the sidewall passivation layer on notch formation or absence (while it is often mentioned that plasma operating conditions and plasma chemistry can be tuned to minimize or even eliminate the notch). Even as Hwang and Giapis[100] explained the mechanisms of notch creation, it seems appropriate to place them in a more global context. In typical ICP gate etching processes based on Cl_2/O_2, HBr/O_2, or $HBr/Cl_2/O_2$ chemistries, passivation layers are formed along the gate sidewalls as etching proceeds; they are thinner at the bottom of the gate as they form from gas-phase deposition of etch by-products.[101] Notch formation is possible only if ions deflected by positive charge built up on the gate oxide can punch through the passivation layer. In this case, Br and Cl radicals generated by the discharge can react with Si on the gate sidewalls and increase the notch depth during the over-etch step of the gate etch process. This hypothesis is reasonable as Cl and Br radicals are no longer loaded by the ion-assisted etching of silicon on the etch front. When the plasma has landed on

the gate oxide, radicals can be consumed only on the silicon sidewalls at the notch location, leading potentially to a very fast increase in notch depth when the passivation layer has been punched through.

The hypothesis holds for notch formation in CW or pulsed plasma even though the combination of low-energy positive ions and negative ions may decrease the potential build-up on the gate oxide when etching is performed in synchronized pulsed mode, thereby decreasing the risk of notch formation. For example, Cunge *et al.*[64] demonstrated that the chemistry of the discharge is altered during the synchronized pulsing mode. In particular, for low duty cycles, the dissociation rate of the feedstock decreases strongly compared to CW conditions. As a result, radical densities in pulsed plasma can be much lower than in a CW plasma, which can significantly limit the risk of notch formation during gate etch processes.[102]

Although etching of magnetic materials involved in spintronics devices is becoming increasingly challenging, pulsed plasmas have seldom been used to etch magnetic materials. Reactive and anisotropic etching of magnetic tunnel junction (MTJ) stacked films, such as the NiFe free layer, pinned CoFe/Ru/CoFe layer, and pinned PtMn layer, using pulsed plasmas has been addressed by Samukawa and co-workers.[103] Their experiments indicated that while corrosion and delamination of MTJs was observed in CW Cl_2 plasmas, neither occurred in a pulsed plasma. They found that the MTJ etch rate increased with peak microwave power when utilizing a pulsed plasma while decreased in a CW plasma as shown in Fig. 17(d). The authors attribute this to the energetic bombardment of negative ions during the after-glow as a consequence of the 600 kHz RF bias on the substrate. This hypothesis is partly supported by Samukawa's earlier observations that the polysilicon etch rate increased in the presence of a 600 kHz RF bias while it remained constant in the presence of 2 MHz RF bias in a pulsed Cl_2 microwave plasma.[30] While the increase in etch rates in pulsed plasma can also be attributed to the increase in bias voltage during the after-glow of the microwave power pulse, a similar increase was not observed for SiO_2 etching. The final etched profiles of an MTJ stack in pulsed Cl_2/Ar and CW Cl_2 plasmas are shown in Fig. 17(a). Anisotropic residue-free profiles are obtained with pulsed plasmas while film delamination and dense corrosion are observed under CW conditions. These observations indicate that pulsed plasma etching is a viable high performance magnetic film processing option for fabricating magnetoresistive random access memory.

Kumagai *et al.*[36] achieved highly anisotropic and corrosion-free PtMn etching with pulsed Cl_2 ECR plasma and a low frequency (600 kHz) bias applied to the wafer. They found that the etch rate increases strongly under pulsed conditions compared to CW and the formation of etch residues and post-etch corrosion products is reduced by extending the after-glow of the time modulated plasma. Increasing the source power also increased the etch rate under pulsed plasma conditions (for an after-glow of $<70\,\mu s$ for a fixed active-glow time of 30 μs) whereas the etch rate decreased in CW plasmas (Fig. 18). Although the increase in etch rate

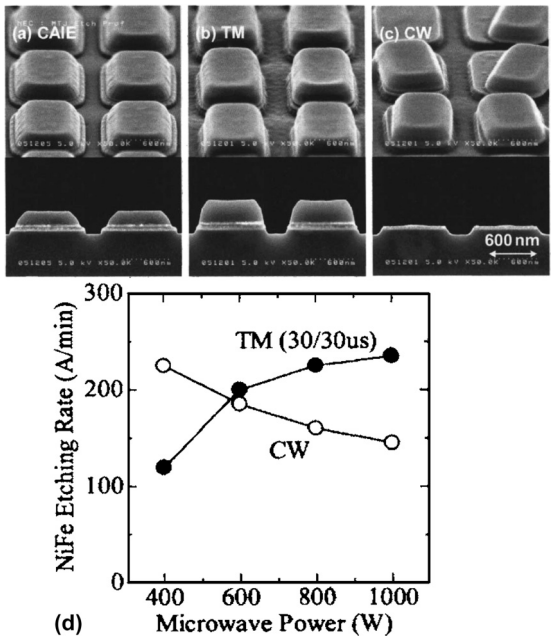

FIG. 17. Etching of magnetic materials using pulsed microwave plasmas. Microwave plasma delivers a peak power of 1 kW and a 600 kHz RF bias at 100 W was applied to the wafer. Profiles of magnetic tunnel junction stacked film (SiO_2 mask-Ta-NiFe-AlO_x-CoFe-Ru-CoFe-PtMn-Ta = 4000/200/50/15/30/10/30/200/200 Å) etched using (a) Cl_2/Ar based chemical assisted ion etching (CAIE), (b) Cl_2 (50 sccm, 2 mTorr) plasma pulsed at 16.67 kHz and 50% duty cycle, and (c) CW Cl_2 plasma. (d) NiFe etching rate in Cl_2 microwave plasma as a function of peak microwave power in CW and plasma pulsed at 50% duty cycle with an active-glow time of 30 μs. Reprinted with permission from T. Mukai, N. Ohshima, H. Hada, and S. Samukawa, J. Vac. Sci. Technol. A **25**, 432 (2007). Copyright 2007, American Vacuum Society.

observed in pulsed plasmas is attributed by the authors to the enhancement of etch reactions promoted by negative ions, the mechanism(s) for the same are not discussed. An analysis of the residual atomic concentrations on the etched surfaces by energy dispersive X-ray fluorescence spectrometry (EDX) revealed that the chlorine concentration on the PtMn surface decreases quite significantly in agreement with the

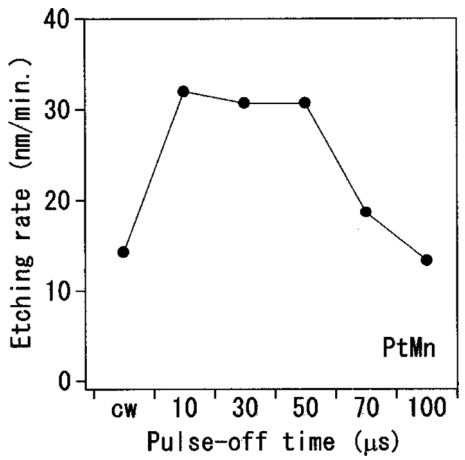

FIG. 18. Etch rate of PtMn in a Cl_2 (50 sccm, 2.025 mTorr, 1000 W) ECR plasma utilizing a 600 kHz RF bias power of 100 W as a function of after-glow time. The active-glow time of the plasma is fixed at 30 μs. Reprinted with permission from S. Kumagai, T. Shiraiwa, and S. Samukawa, J. Vac. Sci. Technol. A **22**, 1093 (2004). Copyright 2004, American Vacuum Society.

global decrease of corrosion observed in pulsed plasmas. However, the total removal of etch residues and corrosion was observed only after H_2-based plasma treatment of etched surfaces.

In the works referenced above, although negative ions are identified as the principal booster of chemical enhanced etching reactions, a more detailed understanding of the exact mechanism is warranted. Indeed, the difference between negative and positive ions in terms of reactive ion etching (RIE) performance is quite unlikely. From Samukawa's results we can only conclude that the after-glow plays a key role during the etching of magnetic materials in pulsed Cl_2 ECR plasmas. Again, the emphasis on the role of negative ions seems unclear as their concentration is lower than that of low-energy positive ions in the after-glow. Instead, the impact on plasma chemistry in pulsed high-density plasma may be more critical.

Cunge *et al.*[64] recently demonstrated that chlorine radical densities decrease in pulsed ICP plasmas (lowering the risk of corrosion as observed by Samukawa and his team). Pulse modulation will also decrease dissociation of etch products in the gas phase (since identical etch rates are obtained even as the total ON time of the plasma is reduced), thereby decreasing re-deposition of etch by-products on the sidewalls. Overall, we acknowledge the potential of pulsed plasmas to improve etch process performance on magnetic materials; however, more work is needed to clearly understand the mechanisms behind the performance benefits.

B. Pulsed plasmas for dielectric etching

The literature for dielectric etching in pulsed ICP or ECR plasmas is much less abundant than that for conductor etching. Samukawa utilized a pulsed ECR plasma to control the polymerization during SiO_2 etching.[81] He employed microwave discharges with varying pulse widths and inter-pulse periods between 10 and 100 μs to control the reactive species density by changing the active-glow and after-glow periods. In particular, CF_2 and F radicals were measured in those experiments using actinometric optical emission spectroscopy. Samukawa[81] found good correlations between the density ratio of CF_2 radicals and F atoms in the CHF_3 plasma and the combination of pulse duration and intervals. The evolution of CF_2 and F densities in the plasmas is discussed in terms of the difference in dissociation rates of the various reaction pathways leading to CF_2 and F radicals. He found that the fluorocarbon polymer content is higher in pulsed discharges relative to the CW discharge, which is attributed to a higher density of F atoms in the plasma relative to CF_x radicals. Indeed, Samukawa[17] found the F-to-CF_2 density ratio to increase with longer active-glow time for a fixed after-glow period of 10 μs (i.e., with increasing duty cycle and lower pulse frequencies). The SiO_2 etch selectivity to Si summarily increased from less than 10 in CW to more than 40 in pulsed conditions, as shown in Fig. 19. However, this contradicts some other observations. For example, the SiO_2 to resist etch selectivity was found to increase from 2 to almost 7 and is attributed to *lower* F atom and *higher* CF_2 densities (i.e., an increase in selectivity was attributed to a *lower* F-to-CF_2 density ratio). The final SEM cross sections of 1 μm SiO_2 contact holes exhibit significant tapering, indicating that polymer deposition by the pulsed plasma is indeed high.[17]

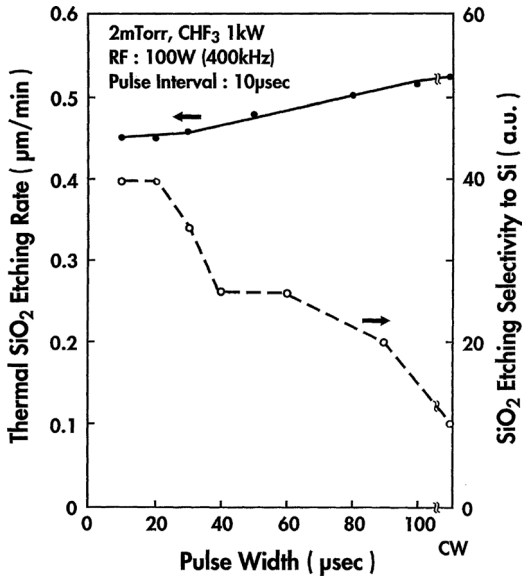

FIG. 19. SiO_2 etching rate and SiO_2/Si selectivity as a function of active-glow duration for a fixed after-glow time of 10 μs in a CHF_3 (20 sccm, 2 mTorr, 1000 W) ECR plasma utilizing a 400 kHz RF bias of 100 W on the wafer. Reprinted with permission from S. Samukawa, Jpn. J. Appl. Phys. **33**, 2133 (1994). Copyright 1994, The Japan Society of Applied Physics.

Schaepkens *et al.*[104] also investigated SiO_2 etching as a function of RF bias frequency and RF bias pulsing. They found that increasing RF bias frequency decreased microtrenching while significantly increasing SiO_2-to-resist etch selectivity. Although bias pulsing frequency did not significantly affect blanket wafer etch rates, pulse duty cycle was found to be important as it determines the time during which etching proceeds (the bias active-glow) and during which fluorocarbon is dominantly deposited at the bottom of trenches (the bias after-glow). They found that the inverse RIE lag effects increased with decreasing duty cycle, which could be explained by the strong aspect ratio dependence of the fluorocarbon deposition rate at the bottom of the features. Similar to Samukawa's results, they also found that SiO_2-to-resist etch selectivity increased with decreasing bias power duty cycle.

Okigawa *et al.*[25] investigated UV damage in fluorocarbon plasmas and its reduction in pulsed plasmas used in charge coupled device (CCD) image sensor wafer processes. UV photon irradiation in these sensors during the etching process presents a number of serious issues, such as increased dark current and interface states. UV absorption at the Si/SiO_2 interface may contribute to a higher density of interface states. During the etching process used to fabricate such devices, the fluorocarbon-film deposition and insulator etching processes must be carefully balanced. Figure 20(a) illustrates the steps involved in micro-lens fabrication. Polymer deposition controls the shape of the micro-lens, while limiting UV radiation is critical for minimizing dark current in

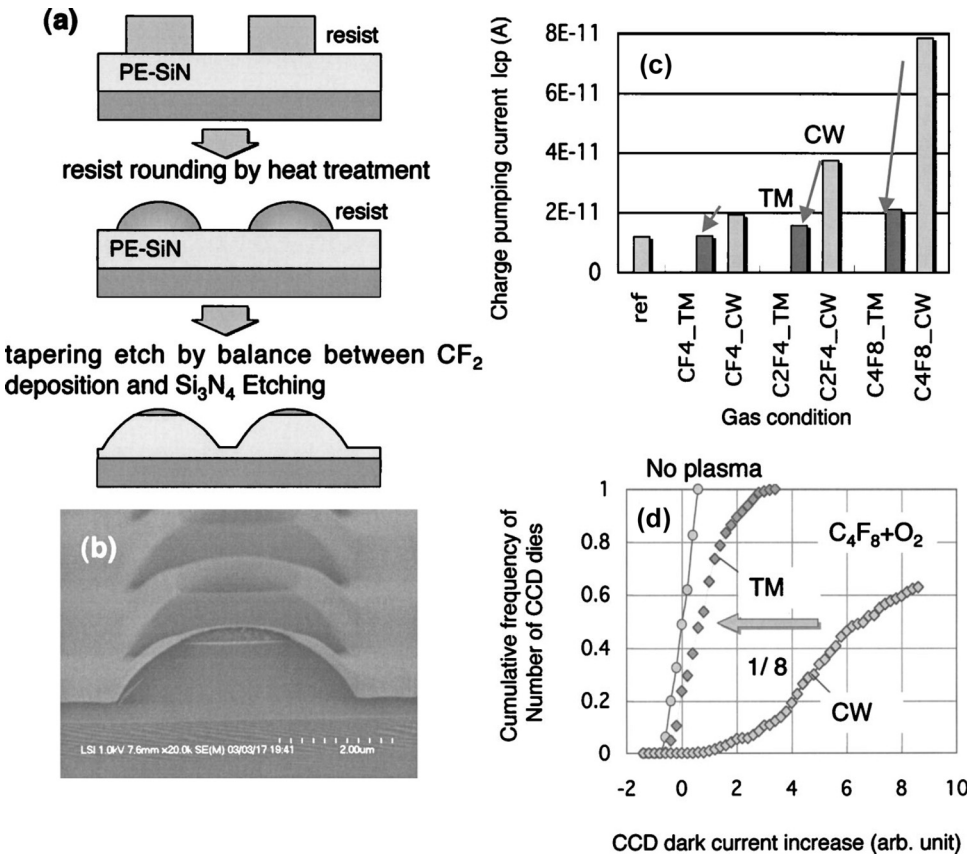

FIG. 20. (a) Formation process for a CCD micro-lens consisting of plasma enhanced silicon nitride (PE-Si_3N_4). (b) Scanning electron micrograph of CCD micro-lenses fabricated by fluorocarbon gas plasma etching. The micro-lens profile is controlled through a balance of CF_2 deposition and Si_3N_4 etching. (c) Comparison of charge pumping current using cw and pulsed plasmas in CF_4, C_2F_4, and C_4F_8. (d) Comparison of CCD dark current in cw and pulsed C_4F_8 plasma. Reprinted with permission from M. Okigawa, Y. Ishikawa, Y. Ichihashi, and S. Samukawa, J. Vac. Sci. Technol. B **22**, 2818 (2004). Copyright 2004, American Vacuum Society.

CCDs. By pulsing the ICP source, both the dark current and interface state density dropped dramatically, as shown in Figs. 20(c) and 20(d), in various plasmas. In particular, the decrease in dark current was found to be highest in C_4F_8 pulsed plasma compared to CF_4 or C_2F_4. Okigawa *et al.*[25] attributed this to the heavier mass of the C_4F_8 molecule, which increases electron energy loss during collisions in the plasma. This decrease is, however, more likely due to the effective reduction in dissociation of the feedstock due to the pulsed plasma nature. As the UV emission is strongest in C_4F_8 CW plasma due to the presence of copious amount of C_xF_y (and CF_2) radicals, pulsing the plasma results in a decrease in their density leading to a significant decrease in UV emission. While the important conclusion from Okigawa *et al.*'s[25] work is that plasma VUV emission is strongly reduced under pulsed plasma conditions compared to CW conditions, more systematic studies of UV emission in different plasma chemistries are required to fully understand the differences among the various fluorocarbon chemistries investigated.

More recently, the effect of bias pulsing on porous SiOCH, SiCH, and SiO_2 etching using pulsed ICP fluorocarbon plasmas was investigated by Raballand *et al.*[101,105] They also found that sensitivity to the pulse frequency was low and that pulse duty cycle strongly influenced both etch rate and selectivity. For example, shortening the duty cycle of the pulsed bias power lowered the etch rate as shown in Fig. 21(a). As etching occurs only when sufficient bias is applied during the etch process, a lower duty cycle decreases the time for which the material is exposed to energetic ion bombardment, leading to a decrease in the average etch rate. In fact, they also observed a shift in the threshold energy for etching toward higher energy as duty cycle decreased.

Raballand *et al.*[105] explain that higher ion energy was required during active-glow to compensate for the absence of energetic ion bombardment during the after-glow of the pulse. This indicates that fluorocarbon polymer deposition increases on all surfaces during the after-glow, necessitating higher bombardment energy during the active-glow to maintain the balance between etching and deposition. They also found that etch selectivity between porous SiOCH and SiCH or SiO_2 improved considerably as the duty cycle decreased [Fig. 21(b)]. While the etching threshold was almost identical for all materials in CW mode, threshold energies for porous SiOCH, SiO_2, and SiCH were all different in the pulsed mode. Consequently, there exists a bias voltage range within which porous SiOCH etching can occur while SiO_2 and SiCH do not etch, yielding, in principle, infinite selectivity. XPS analyses indicated similar CF_x polymer growth on all etched surfaces under CW or pulsed bias conditions. The only difference observed was the

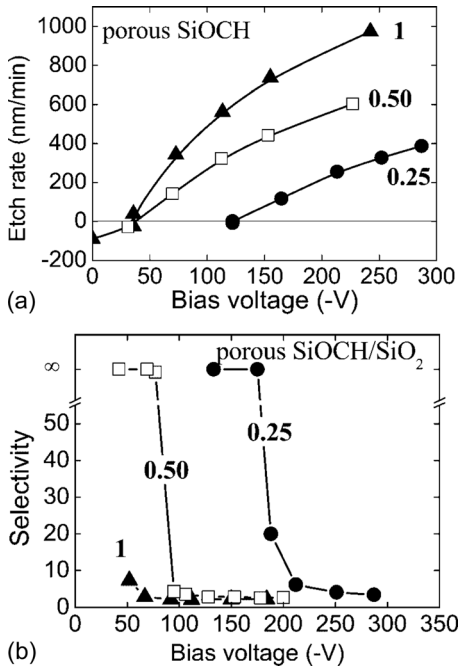

FIG. 21. (a) Impact of the pulsed bias voltage duty cycle (1, 0.50, 0.25) on the porous SiOCH etch rate in CHF_3 plasma. The modulation frequency was fixed at 1 kHz. Decreasing the duty cycle led to a decrease of etch rates and to a shift of the etching/deposition threshold to higher bias voltage. (b) Impact of the pulsed bias voltage duty cycle (1, 0.5, 0.25) on the selectivity between porous SiOCH and SiO_2 in CHF_3 plasma. Reprinted with permission from V. Raballand, G. Cartry, and C. Cardinaud, Plasma Processes Polym. **4**, 563 (2007). Copyright 2005, John Wiley and Sons.

richer fluorine concentration on *p*-SiOCH surfaces. Raballand *et al.*[105] attribute the improvement in selectivity to the lower sensitivity of the porous SiOCH to energetic ion bombardment (as duty cycle decreases, so does the energetic ion bombardment) compared to the denser SiCH and SiO_2.

IV. PULSED PLASMAS FOR INDUSTRIAL PLASMA ETCHING DEVELOPMENT

Albeit demonstrated in academic laboratory scenarios, the discussion so far highlights the potential of pulsed plasmas to improve etch performance in terms of selectivity, PID, aspect ratio dependent etching, charging effect, and profile control. Some of those potential improvements have also been demonstrated in an industrial production tool with pulsed plasma capabilities under industrial high volume manufacturing conditions. However, additional fundamental understanding is necessary to enable the development of manufacturing relevant pulsed plasma processes. Sections IV A–C review recent data gathered on 300 mm diameter wafers under industrially relevant plasma etching conditions in an ICP reactor with pulse capabilities. The reactor details have been discussed earlier in Ref. 22. Although the data presented are only to explain the underlying physics of pulsed plasmas for commonly used etch applications and might not include all details of the processes discussed, the aim is to provide directions and insight for developing processes that benefit to the fullest extent from using pulsed plasmas. Unless otherwise noted below, synchronous pulsing conditions have been used.

A. Surface damage minimization

Minimizing the surface damage induced by plasma etching is one of the major requirements for advanced technological nodes. Etching of most materials introduces a mixed surface layer on top of the surface;[106] a thinner mixed layer is desired to minimize PID. XPS measurements (without air exposure) have been utilized to investigate the surface composition and to estimate the PID in different etching scenarios. For example, Fig. 22 illustrates the surface composition (in atomic percentages) of silicon blanket films when etched in a Cl_2 plasma (20 mTorr, 500 W ICP, 0 W bias) under both CW and pulsed (1 kHz, 10% duty cycle) conditions. Although the surface compositions do not differ significantly, the concentration of oxygen (erosion of reactor walls being one potential source of oxygen[64,65]) is lower under pulsed conditions compared to CW conditions. This indicates that the reactor walls are sputtered more in CW mode than in pulsed mode. To estimate the extent of PID to the silicon film, the full width at half-maximum (FWHM) of the Si-Si XPS peak from the silicon matrix for CW is compared to that for pulsed conditions (see Fig. 23). An increase of the Si(2*p*) FWHM indicates an increase in surface disorder, a measure of the PID. The Si(2*p*) FWHM measured by XPS is 0.59 ± 0.01 eV after exposure to CW Cl_2 plasma, while it is only 0.56 ± 0.01 eV when the Cl_2 plasma is pulsed at 1 kHz and 10% duty cycle. This indicates that the plasma in CW mode produces a thicker mixed layer and increased amorphization of the surface. As pulsing the plasma limits the surface mixing, less damage is expected to the materials during plasma exposure.

Silicon etching in CW HBr/O_2 plasma during the gate over-etch process achieves very high selectivity to SiO_2. However, ion-induced diffusion pathways in the oxide and diffusion/implantation of oxygen, water, and bromine results in oxidation of the underlying silicon.[107–109] Recently, Darnon *et al.*[110] and Petit-Etienne *et al.*[111] showed that pulsing the plasma at a low duty cycle and high frequency strongly

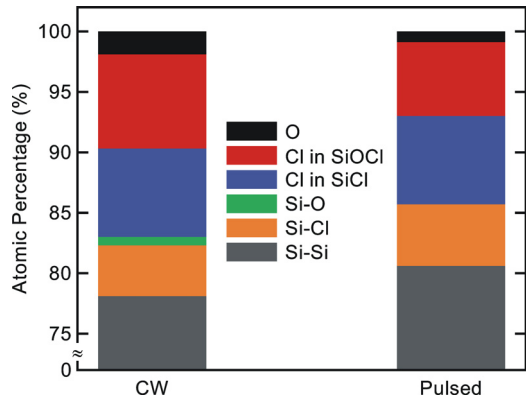

FIG. 22. (Color online) Surface composition of Si exposed to continuous wave and synchronous pulsed plasma at 1 kHz, 10% duty cycle. Si-Si contribution is not presented.

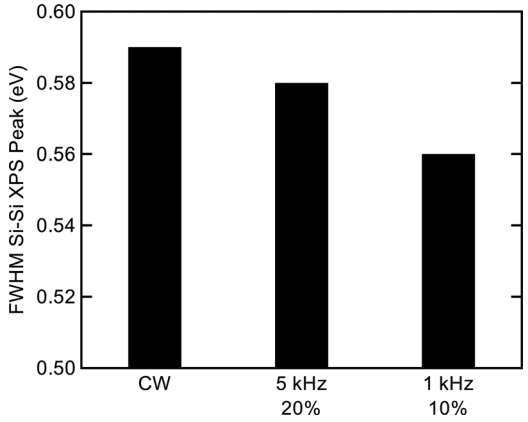

FIG. 23. FWHM of the Si-Si XPS peak measured by XPS at 45° photoelectron take-off angle for Si exposed to CW and synchronous pulsed Cl_2 plasma.

decreases the amount of plasma induced oxidation, as shown in Fig. 24. This is attributed to the difference in ion composition, which is more molecular in pulsed plasma and more atomic in CW plasmas. Consequently, for similar ion energies, the energy per ion component is lower in pulsed plasmas, thereby decreasing the damage.

During high-k metal gate etching, silicon recess and damage in the source/drain region during etching must also be minimized. In Ar/BCl_3 plasma, infinite HfO_2 selectivity over SiO_2 or Si is obtained owing to the formation of the BCl_x polymer exclusively on the top Si or SiO_2 surface during the process.[112,113] The precursors for polymer growth originate from the gas-phase dissociation of BCl_3. When the plasma is pulsed, the source of polymer precursors is strongly attenuated. As a consequence, a transition from deposition to etching is observed, leading to a loss in selectivity. An example of such a transition for plasmas sustained in Ar/BCl_3 is shown in Fig. 25. While polymer growth on SiO_2 was observed

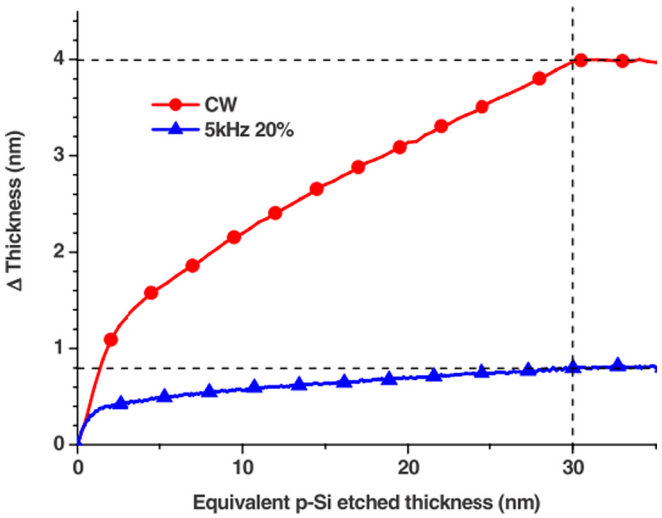

FIG. 24. (Color online) Damage penetration measured by kinetic *in situ* ellipsometry as a function of equivalent poly-Si etched thickness in CW and synchronous pulsing mode at 5 kHz and 20% duty cycle. Reprinted with permission from C. Petit-Etienne *et al.*, J. Vac. Sci. Technol. B **28**, 926 (2010). Copyright 2010, American Vacuum Society.

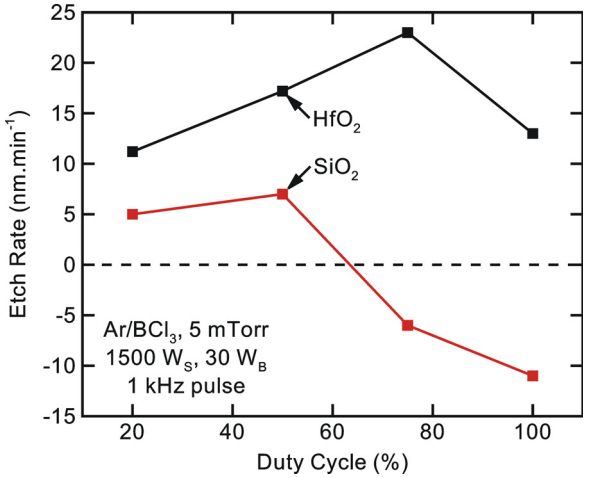

FIG. 25. (Color online) Time compensated etch rate of blanket SiO_2 and HfO_2 films as a function of the pulse duty cycle in etch-inhibitor regime (BCl_3/Ar/5 mT/1500 Ws/30 Wb/1 kHz—synchronous pulsing).

under CW conditions, no such buildup was observed during pulsing, resulting in SiO_2 etch. The decrease in precursor density also affects HfO_2 etching. For example, the HfO_2 etch rate is slightly affected when the plasma is pulsed, leading to an increase in etch rate at low duty cycles due to lack of polymer precursors to inhibit etching.

When developing an etch process under pulsed plasma conditions, the CW process baseline may have to be tuned to realize all the benefits of pulsed plasma. By varying the gas feed and plasma operating parameters, infinite selectivity can be recovered in pulsed mode. In this case, XPS analysis of the Si peaks after HfO_2 etching in BCl_3/Ar indicates a decrease of silicon amorphization in pulsed versus CW plasma. In the experimental conditions (200 BCl_3, 200 Ar, 5 mTorr, 1500 W ICP power, 30 W bias, synchronous pulsing 1 kHz), the Si($2p$) peak FWHM decreases to 0.6 eV when the plasma is pulsed compared to 0.8 eV when the plasma is in CW mode. The Si($2p$) peak FWHM measured after exposure to the pulsed BCl_3 plasma is very close to the reference measured on Si after HF dip (0.55 eV). This indicates that pulsed Ar/BCl_3 plasma induces very little amorphization of the silicon substrate. Hence, pulsing the plasma for metal-gate high-k etching processes is also a promising way to prevent Si amorphization in the source-drain region.

B. Uniformity control

Recent papers have also shown that pulsing the plasma may have a huge impact on etch uniformity, which is of paramount importance for large-scale wafer processing. For example, Banna *et al.*[22] and Tokashiki *et al.*[4] have shown that the etch rate *nonuniformity* is halved when plasma is pulsed synchronously. The improvement in uniformity is attributed to ion and neutral relaxation during the after-glow. In addition, gas convection caused by the drop in electron pressure during the after-glow plays a significant role in increasing radical density uniformity within the plasma, thereby improving the etch rate uniformity.[77]

C. Patterned structure etching: Profile evolution

In the following, we consider a typical STI etch process to illustrate the impact of synchronous pulsed plasma on profile evolution. It should be noted that the CW baseline was intentionally not fully optimized in order to better understand the impact of pulsed plasmas on etching of patterned structures when performing one-to-one process transfer without any additional tuning. We re-emphasize that process tuning is key to achieving the best performance due to the differences in the plasma nature under CW and pulsed conditions. While we illustrate the differences in the etch mechanism, it is beyond the focus of this discussion to present fully optimized conditions for either plasma state.

Figure 26 illustrates silicon patterns etched in CW and pulsed HBr/O_2 plasmas. The etched pattern in pulsed plasma has significantly better characteristics than those etched using the CW plasma. Not only does the amorphous carbon hard mask exhibit significantly less faceting but the sidewall angles are also more vertical under pulsed conditions. Further, the profile differences between semi-isolated and dense lines are strongly minimized under pulsed conditions. The decrease in mask faceting is attributed to an increase in surface passivation via reactive radicals and less sputtering by ions during the after-glow when ions arrive with only low energies. Overall, pulsed plasma conditions seem to provide a much tighter critical dimension distribution for all pattern types (isolated and dense) within a die. Experiments for varying duty cycles and pulse frequencies indicate that the profile improvements are dominantly determined by duty cycle and not by the pulse frequency. In particular, plasma pulsing at lower duty cycles significantly improves etch profiles. In summary, under pulsed plasma conditions the process shifts toward a leaner, less polymerizing chemistry.

The more vertical sidewalls and better iso-dense critical dimension uniformity indicates a decrease in deposition on the sidewalls in pulsed conditions and particularly so at lower duty cycles. This is confirmed by the passivation thickness profiles shown in Fig. 27 for 20 nm STI trenches under both pulsed and CW conditions.[114] A thicker layer is created on the sidewall of isolated patterns etched in CW mode than in pulsed mode. Furthermore, clogging at the top of the trench is observed in CW mode, as shown in Fig. 27(a). The clogging is attributed to the accumulation of etch by-products that oxidize (due to the oxygen radicals, the flux of which is highest near the top of the trench) as they leave the narrow trenches.

The lack of clogging and thinner passivation layers under pulsed conditions can be attributed to several factors:

(1) The lower average etch rate in pulsed plasmas decreases the flux of etch by-products in the gas phase. As these by-products contribute to the passivation layer, their lower flux results in thinner passivation layers and, therefore, to less clogging.
(2) The lower dissociation fraction in pulsed plasma decreases the density of O radicals responsible for oxidation of the etch by-products near the top of the trench and on the patterned sidewalls.
(3) The lower dissociation fraction also results in decreased fragmentation of etch by-products, thereby retaining their volatility.
(4) Spontaneous etching of silicon by reactive radicals arriving during the after-glow.
(5) Less physical etching as a result of higher molecular ion density compared to atomic ions in CW plasmas. The heavier molecular ions typically have lower energy per component, which results in less sputtering.

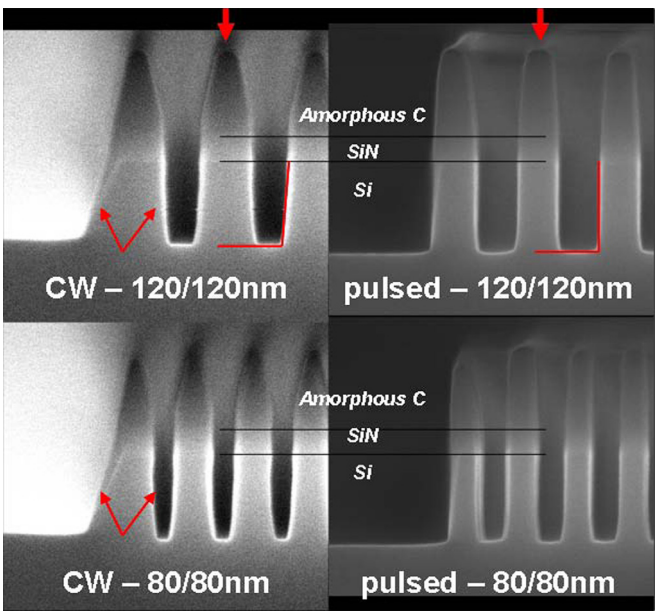

FIG. 26. (Color online) 120 nm-wide with space of 120 and 80 nm—wide with a space of 80 nm trenches etched in silicon in optimized HBr/O_2 plasma for both CW and synchronous pulsing modes.

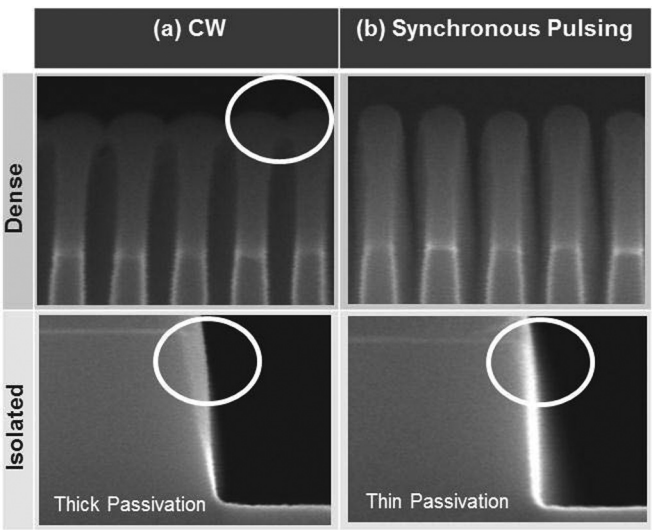

FIG. 27. Sub-20 nm trenches etched in HBr/O_2 etch processes using (a) CW condition and (b) synchronous pulsed condition. Thin passivation layers are formed on the sidewalls of isolated lines under the pulsed mode while thicker passivation layers are formed in CW mode. Top clogging of trenches is observed in CW condition (from Ref. 114).

Such improvements in profile characteristics have also been observed for patterns with SiO_2 hard-mask. For example, structures with varying critical dimensions of 40–100 nm etched using CW and pulsed plasmas are shown in Fig. 28. Clearly, profiles etched under pulsed plasma conditions exhibit significantly higher mask selectivity with less faceting while the passivation layer on the sidewall is also more uniform. The etch process does, however, require further tuning as the bottom of the trenches thus etched exhibit micro-trenching under pulsed conditions. This phenomenon is quite unexpected as HBr/O_2 plasmas are known to etch without micro-trenching effects compared to, for example, Cl_2 based plasmas.

Comparison of pattern profiles etched under CW and pulsed plasma conditions have demonstrated the high potential of plasma pulsing for pattern control. The variations in ion/radical flux and ion energy during pulsing results in significant profile differences. Pulsed plasmas generate profiles with more vertical sidewalls, better iso/dense CD uniformity, and significantly less mask erosion. The duty cycle is the major control parameter for profile tuning while pulsing frequency has little impact. However, pulsing the plasma (while keeping all other operating parameters constant) may also yield some nonideal profile characteristics, such as micro-trenching. This reinforces the vital importance of process tuning in achieving excellent profile control.

V. FUTURE DIRECTIONS AND CHALLENGES

A. Future outlook

Many of the advantages of pulsed plasmas in designing plasma etch processes are derived from two new parameters: pulse frequency and duty cycle. Although addition of these new control knobs increases the complexity of an already complex environment under CW conditions, they also increase the flexibility with which one can design etch processes to achieve the level of precision and control required for further device scaling. Most of the conclusions drawn by the literature available on pulsed plasmas pertain to variations in gas-phase dynamics during pulsing. At least two important characteristics of pulsed plasmas play a role in process design:

(1) Pulsed plasmas exhibit lower fragmentation (while maintaining a decent ion flux and energy during the on-time); the lower concentration of reactive radicals minimizes all undesired etch profile characteristics, such as bowing, undercut, and notching, while less fragmentation of etch by-products leads to lower re-deposition of nonvolatile species on the wafer during the etch process.
(2) Pulsed plasmas comprised of more "molecular" than "atomic" species; this is true for neutral species as well as ions. As molecular ions fragment upon surface impact, the energy splitting leads to less energetic particles. From the process point of view, two important consequences have been reported. First, mask erosion is minimized (less vertical etch and faceting) even for processes utilizing high bias power on the wafer. Second, less ion-induced damage (both physical and chemical) of ultra-thin layers occurs, which reduces recess into the substrate material when very low (to none) bias power is applied to the wafer.

As the devices envisioned for the sub-10 nm technology node are FinFET and FDSOI (fully depleted silicon on insulator) transistors, pulsed plasmas must demonstrate improvement in etching of such devices.[115–117] FinFET transistor fabrication (either gate-first or gate-last) is challenging as etch processes must accommodate complex topography created by the fin.[118,119] In the gate-last approach, the silicon of the dummy gate must be etched without damaging the fin, which is protected only by an ultra-thin SiO_2 layer (less than a few nanometers). Further, the top surface of the fin is exposed to the dummy-gate etch process while the dummy gate is removed along the fin sidewalls. Faceting of the fin can occur during dummy-gate etching in CW plasmas even when using moderate ion energies. In the gate-first approach, the top surface may exhibit faceting when removing the metal and high-*k* dielectrics from the top and the sidewalls of the fin. Synchronous pulsed plasmas, which generate molecular ions, can minimize the chemically enhanced (due to

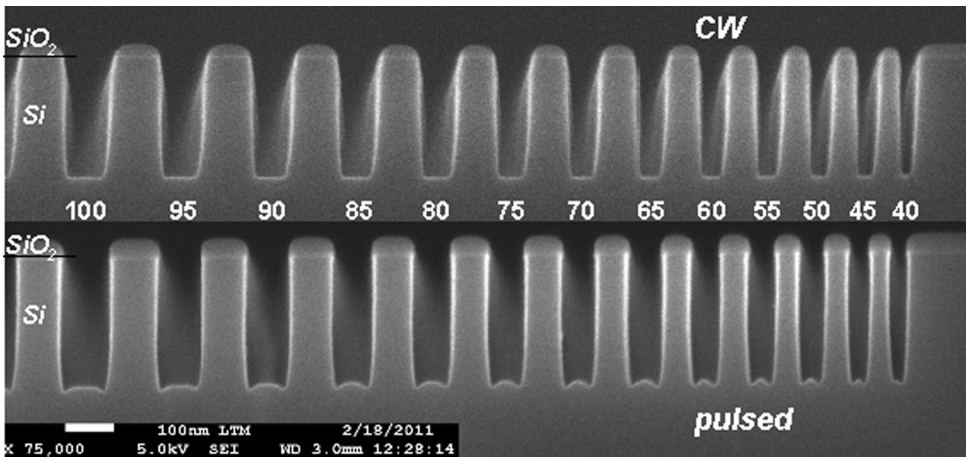

FIG. 28. Array of Si trenches with various widths etched in silicon with SiO_2 hard-mask in HBr/O_2 plasma in CW and synchronous pulsing mode at 1 kHz 20% duty cycle.

energy splitting) erosion rate of the fin responsible for the faceting. For example, 40 eV Cl_2^+ splits into two 20 eV Cl radicals upon impact on the fin surface. For either approach, spacer patterning can similarly benefit from plasma pulsing as the top of the fin can be damaged and eroded when the spacer material is removed from the fin sidewalls.

FDSOI devices, the most serious alternative to FinFET devices, also suffer from significant integration issues.[117] The critical challenge is to minimize the consumption of the ultra-thin crystalline silicon layer (on the order of 5 nm) on which the device is built. In a gate-first approach, silicon recess occurs during high-k etching as well as spacer etching. Using a CW etch process with very low bias power, a silicon recess of, at best, 3 nm can be achieved while no silicon consumption is allowed for the raised source/drain epitaxial silicon regrowth. In this situation, the less energetic ions in pulsed plasmas can minimize the recess. This effect has already been observed during high-k etching in BCl_3 plasmas and when gate etch plasmas land on an ultra-thin SiO_2 layer. Similar results are expected during nitride spacer etching for FDSOI as well as for FinFET devices.

Another aspect of processing for which pulsed plasmas may be beneficial is maintaining the integrity of the photoresist. Indeed, for front end of line as well as back end of line applications, resists and fragile multilayer hard mask schemes are mandatory. Currently, 193 nm resists are used to open a silicon-containing layer (imposed by the 193 nm lithographic step) followed by patterning hard mask layers (typically SiO_2 and amorphous carbon layers). Current CW processes used to open silicon-containing layers employ fluorocarbon-based plasmas that lead to roughness and striations attributed to the stress induced by interaction between the fluorocarbon layer and the photoresist. Owing to its molecular ion composition and lower fragmentation of the fluorocarbon feedstock, pulsed plasma demonstrates improved selectivity to the mask. We anticipate reduction in both roughness and striation while maintaining, at least, the selectivity to the resist.

Advanced patterning technologies, such as double, triple, or quadruple patterning, may also benefit from pulsed plasmas. In these applications, faceting during spacer etch may lead to critical dimension nonuniformities between pairs and bowing due to ion reflection on the spacer facets. Pulsed plasmas can improve critical dimension control and patterning performance as their less energetic molecular ions cause less faceting of the spacer and thus bowing of the profile.

B. Challenges and concluding remarks

Time modulation (pulsing) of high-density plasmas appears to be a promising approach by which the growing need for flexible control of plasma properties to address the increasingly stringent and conflicting requirements in microelectronics can be achieved. In this work, we reviewed the fundamental physics underlying the etching mechanisms in pulsed high-density plasmas. In particular, we discussed the impact of pulse parameters (frequency, duty cycle, and phase lag) on the dynamics of charged species and radicals in typical etching processes. We summarized research over the past three decades on pulsed plasmas for advanced etching applications in an attempt to provide general guidance for process development and optimization under such an operating regime.

Based on these discussions, the potential benefits of pulsed plasma for advanced dry etching processes can be categorized into four different aspects:

1. Plasma chemistry

(1) Adjust the fluxes of reactive species impinging the wafer surface.
(2) Control dissociation rate and polymer formation.
(3) Minimize etch by-product re-deposition at the feature sidewalls.

2. Feature profile characteristics

(1) Reduce profile distortion, such as notching, bowing, and micro-trenching.
(2) Improve macroscopic and microscopic uniformities as well as selectivity.
(3) Control dense-to-isolated feature micro-loading.

3. PID

(1) Reduce charge build-up damage.
(2) Reduce average ion energy bombardment, UV, and VUV radiation.
(3) Control breakdown voltage or threshold voltage shift.

4. Process design flexibility

(1) Improve control of key plasma characteristics (ion energy and angular distributions, electron temperature, and radical-to-ion flux ratio).
(2) Additional process control knobs (pulse frequency, pulse duty cycle, and phase lag between source and bias pulses for synchronous pulsing mode).
(3) Widen process window of conditions for stable plasma operation.

Such flexibility also increases the complexity in process design, primarily due to the different nature of pulsed plasma, compared to its CW counterpart, for which the industry has developed extensive expertise over the past three decades. Hence, in most cases, process tuning will be required after a one-to-one baseline transfer from CW to pulsed mode. As the key plasma characteristics do not scale linearly with pulse frequency and duty cycle due to their nonlinear interaction, very extensive screening tests for different processes are in progress to most effectively realize the enormous potential of using pulsed plasmas. The multiple schemes of available pulsed plasma modes (source, bias, synchronous, and embedded pulsing) are additional variables in an already large parameter space. Optimized pulse conditions must be carefully selected to satisfy process requirements ranging from basic etch criteria (e.g., selectivity, loading, and profile) to increasingly specialized specifications for complex advanced devices and interconnect structures.

To assist in implementing plasma pulsing and facilitate related process tuning, we have provided a detailed account of trends in the application of pulsed plasma and future directions for advanced dry etching processes. In particular, differences between the multiple pulsing schemes were reviewed. Deeper scientific understanding of the fundamentals will help guide today's industrial process engineers to efficiently realize the full potential of pulsed plasmas in a very large parameter space that faces increasingly challenging performance demands.

ACKNOWLEDGMENTS

This work was supported by the Applied Materials University Research Partnership Program. The authors would like to thank the extended pulsed plasma development teams (hardware and process engineers) at Applied Materials Inc. and CNRS-LTM for their contributions.

[1]M. A. Lieberman and A. J. Lichtenberg, *Principles of Plasma Discharges and Materials Processing* (John Wiley & Sons, Inc., Hoboken, NJ, 2005).
[2]*Handbook of Semiconductor Manufacturing Technology*, edited by R. Doering and Y. Nishi, 2nd ed. (CRC Press, Cleveland, OH, 2007).
[3]P. Chabert and N. Braithwaite, *Physics of Radio-Frequency Plasmas* (Cambridge University Press, Cambridge, 2011).
[4]K. Tokashiki, *et al*., Jpn. J. Appl. Phys. **48**, 08HD01 (2009).
[5]K. P. Cheung and C. P. Chang, J. Appl. Phys. **75**, 4415 (1994).
[6]S. Fang, S. Murakawa, and J. P. McVittie, IEEE Trans. Electron Devices **41**, 1848 (1994).
[7]T. Tokashiki, K. Noguchi, K. Miyamoto, and H. Horiuchi, in *Plasma Process-Induced Damage*, 2nd International Symposium, p. 207 (1997).
[8]T. Yunogami, T. Mizutani, K. Suzuki, and S. Nishimatsu, Jpn. J. Appl. Phys. **28**, 2172 (1989).
[9]K. Hashimoto, Jpn. J. Appl. Phys. **33**, 6013 (1994).
[10]T. Tatsumi, S. Fukuda, and S. Kadomura, Jpn. J. Appl. Phys. **33**, 2175 (1994).
[11]S. Sakamori, T. Maruyama, N. Fujiwara, and H. Miyatake, Jpn. J. Appl. Phys. **37**, 2321 (1998).
[12]K. Yonekura, T. Katayama, T. Maruyama, N. Fujiwara, and H. Miyatake, J. Vac. Sci. Technol. A **18**, 176 (2000).
[13]J. Kim, K. S. Shin, W. J. Park, Y. J. Kim, C. J. Kang, T. H. Ahn, and J. T. Moon, J. Vac. Sci. Technol. A **19**, 1835 (2001).
[14]G. S. Hwang and K. P. Giapis, Jpn. J. Appl. Phys. **37**, 2291 (1998).
[15]S. Samukawa and K. Terada, J. Vac. Sci. Technol. B **12**, 3300 (1994).
[16]S. Samukawa, Appl. Phys. Lett. **64**, 3398 (1994).
[17]S. Samukawa, Jpn. J. Appl. Phys. **33**, 2133 (1994).
[18]A. Yokozawa, H. Ohtake, and S. Samukawa, Jpn. J. Appl. Phys. **35**, 2433 (1996).
[19]S. Samukawa, H. Ohtake, and T. Mieno, J. Vac. Sci. Technol. A **14**, 3049 (1996).
[20]T. H. Ahn, K. Nakamura, and H. Sugai, Plasma Sources Sci. Technol. **5**, 139 (1996).
[21]T. Mieno and S. Samukawa, Plasma Sources Sci. Technol. **6**, 398 (1997).
[22]S. Banna, *et al*., IEEE Trans. Plasma Sci. **37**, 1730 (2009).
[23]A. Agarwal, P. J. Stout, S. Banna, S. Rauf, K. Tokashiki, J.-Y. Lee, and K. Collins, J. Appl. Phys. **106**, 103305 (2009).
[24]M. Okigawa, Y. Ishikawa, and S. Samukawa, J. Vac. Sci. Technol. B **21**, 2448 (2003).
[25]M. Okigawa, Y. Ishikawa, Y. Ichihashi, and S. Samukawa, J. Vac. Sci. Technol. B **22**, 2818 (2004).
[26]R. W. Boswell and D. Henry, Appl. Phys. Lett. **47**, 1095 (1985).
[27]S. Samukawa and S. Furuoya, Appl. Phys. Lett. **63**, 2044 (1993).
[28]H. Ohtake and S. Samukawa, Appl. Phys. Lett. **68**, 2416 (1996).
[29]S. Samukawa and T. Mieno, Plasma Sources Sci. Technol. **5**, 132 (1996).
[30]S. Samukawa, Appl. Phys. Lett. **68**, 316 (1996).
[31]J. T. Verdeyen, J. Vac. Sci. Technol. A **8**, 1851 (1990).
[32]C. Grabowski and J. M. Gahl, J. Appl. Phys. **70**, 1039 (1991).
[33]L. J. Overzet, Y. Lin, and L. Luo, J. Appl. Phys. **72**, 5579 (1992).
[34]L. J. Overzet, B. A. Smith, J. Kleber, and S. K. Kanakasabapathy, Jpn. J. Appl. Phys. **36**, 2443 (1997).
[35]S. K. Kanakasabapathy, L. J. Overzet, V. Midha, and D. Economou, Appl. Phys. Lett. **78**, 22 (2001).
[36]S. Kumagai, T. Shiraiwa, and S. Samukawa, J. Vac. Sci. Technol. A **22**, 1093 (2004).
[37]H. Ohtake, K. Noguchi, S. Samukawa, H. Iida, A. Sato, and X.-Y. Qian, J. Vac. Sci. Technol. B **18**, 2495 (2000).
[38]V. Todorow, J. Holland, and N. Gani, U.S. patent 6818562 (16 November 2004).
[39]J.-Y. Chen, J. P. Holland, A. H. Sato, and V. N. Todorow, U.S. patent 6472822 (29 October 2002).
[40]S. Banna, V. Todorow, and K. Ramaswamy, U.S. patent 0284156 A1 (19 November 2009).
[41]A. Agarwal, *et al*., Appl. Phys. Lett. **100**, 044105 (2012).
[42]S. Ashida, C. Lee, and M. A. Lieberman, J. Vac. Sci. Technol. A **13**, 2498 (1995).
[43]D. P. Lymberopoulos, V. I. Kolobov, and D. J. Economou, J. Vac. Sci. Technol. A **16**, 564 (1998).
[44]P. Subramonium and M. J. Kushner, J. Vac. Sci. Technol. A **20**, 313 (2002).
[45]P. Subramonium and M. J. Kushner, J. Appl. Phys. **96**, 82 (2004).
[46]M. A. Lieberman and S. Ashida, Plasma Sources Sci. Technol. **5**, 145 (1996).
[47]S. Behle, A. Brockhaus, and J. Engemann, Plasma Sources Sci. Technol. **9**, 57 (2000).
[48]H. Sugai, K. Nakamura, Y. Hikosaka, and M. Nakamura, J. Vac. Sci. Technol. A **13**, 887 (1995).
[49]M. V. Malyshev, V. M. Donnelly, J. I. Colonell, and S. Samukawa, J. Appl. Phys. **86**, 4813 (1999).
[50]T. Mieno and S. Samukawa, Jpn. J. Appl. Phys. **34**, L1079 (1995).
[51]M. Edamura, E. C. Benck, and Y. Wang, J. Vac. Sci. Technol. A **24**, 2151 (2006).
[52]D. Hayashi and K. Kadota, J. Appl. Phys. **83**, 697 (1998).
[53]H. M. Katsch, C. Manthey, and H. F. D. Bele, Plasma Sources Sci. Technol. **12**, 475 (2003).
[54]S. Ashida and M. A. Lieberman, Jpn. J. Appl. Phys. **36**, 854 (1997).
[55]M. Meyyappan, J. Vac. Sci. Technol. A **14**, 2122 (1996).
[56]E. G. Thorsteinsson and J. T. Gudmundsson, J. Phys. D: Appl. Phys. **43**, 115202 (2010).
[57]V. Midha and D. J. Economou, Plasma Sources Sci. Technol. **9**, 256 (2000).
[58]P. Subramonium and M. J. Kushner, Appl. Phys. Lett. **79**, 2145 (2001).
[59]B. Ramamurthi and D. J. Economou, J. Vac. Sci. Technol. A **20**, 467 (2002).
[60]S. Kim, M. A. Lieberman, A. J. Lichtenberg, and J. T. Gudmundsson, J. Vac. Sci. Technol. A **24**, 2025 (2006).
[61]S. Panda, D. J. Economou, and M. Meyyappan, J. Appl. Phys. **87**, 8323 (2000).
[62]M. Meyyappan, Jpn. J. Appl. Phys. **36**, 4820 (1997).
[63]R. W. Boswell and D. Vender, IEEE Trans. Plasma Sci. **19**, 141 (1991).
[64]G. Cunge, D. Vempaire, R. Ramos, M. Touzeau, O. Joubert, P. Bodard, and N. Sadeghi, Plasma Sources Sci. Technol. **19**, 034017 (2010).
[65]A. Agarwal and M. J. Kushner, J. Vac. Sci. Technol. A **26**, 498 (2008).
[66]O. Zabeida and L. Martinu, J. Appl. Phys. **85**, 6366 (1999).
[67]G. D. Conway, A. J. Perry, and R. W. Boswell, Plasma Sources Sci. Technol. **7**, 337 (1998).
[68]O. Zabeida, A. Hallil, M. R. Wertheimer, and L. Martinu, J. Appl. Phys. **88**, 635 (2000).
[69]S. A. Voronin, M. R. Alexander, and J. W. Bradley, Meas. Sci. Technol. **16**, 2446 (2005).
[70]Y. Wang, E. C. Benck, M. Misakian, M. Edamura, and J. K. Olthoff, J. Appl. Phys. **87**, 2114 (2000).
[71]M. V. Malyshev and V. M. Donnelly, Plasma Sources Sci. Technol. **9**, 353 (2000).
[72]P. Subramonium and M. J. Kushner, J. Vac. Sci. Technol. A **22**, 534 (2004).
[73]A. Agarwal, P. J. Stout, S. Banna, S. Rauf, and K. Collins, J. Vac. Sci. Technol. A **29**, 011017 (2011).
[74]S. G. Walton, D. Leonhardt, R. F. Fernsler, and R. A. Meger, Appl. Phys. Lett. **81**, 987 (2002).
[75]K. S. Shin, K. K. Chi, C. J. Kang, C. Jung, C. O. Jung, J. T. Moon, and M. Y. Lee, Jpn. J. Appl. Phys. **37**, 2349 (1998).

[76]A. Agarwal, S. Rauf, and K. Collins, IEEE Trans. Plasma Sci. **39**, 2520 (2011).
[77]G. Cunge, D. Vempaire, and N. Sadeghi, Appl. Phys. Lett. **96**, 131501 (2010).
[78]G. Cunge, M. Mori, M. Kogelschatz, and N. Sadeghi, Appl. Phys. Lett. **88**, 051501 (2006).
[79]G. Cunge, N. Sadeghi, and R. Ramos, J. Appl. Phys. **102**, 093304 (2007).
[80]P. Bodart, M. Brihoum, G. Cunge, O. Joubert, and N. Sadeghi, J. Appl. Phys. **110**, 113302 (2011).
[81]S. Samukawa, Jpn. J. Appl. Phys. **32**, 6080 (1993).
[82]K. Takahashi, M. Hori, and T. Goto, Jpn. J. Appl. Phys. **32**, L1088 (1993).
[83]S. Hayashi, H. Nakagawa, M. Yamanaka, and M. Kubota, Jpn. J. Appl. Phys. **36**, 4845 (1997).
[84]M. Yamanaka, S. Hayashi, M. Kubota, and H. Nakagawa, Jpn. J. Appl. Phys. **37**, 2343 (1998).
[85]J. P. Booth, G. Cunge, P. Chabert, and N. Sadeghi, J. Appl. Phys. **85**, 3097 (1999).
[86]J. P. Booth, H. Abada, P. Chabert, and D. B. Graves, Plasma Sources Sci. Technol. **14**, 273 (2005).
[87]J. P. Booth, G. Hancock, N. D. Perry, and M. J. Toogood, J. Appl. Phys. **66**, 5251 (1989).
[88]G. Cunge and J. P. Booth, J. Appl. Phys. **85**, 3952 (1999).
[89]G. Cunge, P. Chabert, and J.-P. Booth, Plasma Sources Sci. Technol. **6**, 349 (1997).
[90]G. Cunge, P. Chabert, and J.-P. Booth, J. Appl. Phys. **89**, 7750 (2001).
[91]G. Cunge, D. Vempaire, M. Touzeau, and N. Sadeghi, Appl. Phys. Lett. **91**, 231503 (2007).
[92]C. S. Moon, K. Takeda, S. Takashima, M. Sekine, Y. Setsuhara, M. Shiratani, and M. Hori, J. Appl. Phys. **107**, 103310 (2010).
[93]P. Bodart, *et al*., in *4th International Workshop on Plasma Etch and Strip in Microelectronics* (Mechelen, Belgium, 2011).
[94]M. Haass, M. Darnon, E. Pargon, S. Banna, and O. Joubert, in *63rd Gaseous Electronics Conference* (Paris, France, 2010).
[95]D. Vempaire and G. Cunge, Appl. Phys. Lett. **94**, 021504 (2009).
[96]R. W. Boswell and R. K. Porteous, J. Appl. Phys. **62**, 3123 (1987).
[97]R. Petri, B. Kennedy, D. Henry, N. Sadeghi, and J.-P. Booth, J. Vac. Sci. Technol. B **12**, 2970 (1994).
[98]L. J. Overzet, J. H. Beberman, and J. T. Verdeyen, J. Appl. Phys. **66**, 1622 (1989).
[99]T. Maruyama, N. Fujiwara, S. Ogino, and H. Miyatake, Jpn. J. Appl. Phys. **37**, 2306 (1998).
[100]G. S. Hwang and K. P. Giapis, J. Vac. Sci. Technol. B **15**, 70 (1997).
[101]V. Raballand, G. Cartry, and C. Cardinaud, J. Appl. Phys. **102**, 063306 (2007).
[102]R. Ramos, G. Cunge, and O. Joubert, Vacuum **25**, 290 (2007).
[103]T. Mukai, N. Ohshima, H. Hada, and S. Samukawa, J. Vac. Sci. Technol. A **25**, 432 (2007).
[104]M. Schaepkens, G. S. Oehrlein, and J. M. Cook, J. Vac. Sci. Technol. B **18**, 856 (2000).
[105]V. Raballand, G. Cartry, and C. Cardinaud, Plasma Processes Polym. **4**, 563 (2007).
[106]J. J. Végh, D. Humbird, and D. B. Graves, J. Vac. Sci. Technol. A **23**, 1598 (2005).
[107]L. Vallier, L. Desvoivres, M. Bonvalot, and O. Joubert, Appl. Phys. Lett. **75**, 1069 (1999).
[108]V. M. Donnelly, F. P. Klemens, T. W. Sorsch, G. L. Timp, and F. H. Baumann, Appl. Phys. Lett. **74**, 1260 (1999).
[109]S. A. Vitale and B. A. Smith, J. Vac. Sci. Technol. B **21**, 2205 (2003).
[110]M. Darnon, *et al*., ECS Trans. **27**, 717 (2010).
[111]C. Petit-Etienne, *et al*., J. Vac. Sci. Technol. B **28**, 926 (2010).
[112]L. Sha and J. P. Chang, J. Vac. Sci. Technol. A **22**, 88 (2004).
[113]E. Sungauer, E. Pargon, X. Mellhaoui, R. Ramos, G. Cunge, L. Vallier, O. Joubert, and T. Lill, J. Vac. Sci. Technol. B **25**, 1640 (2007).
[114]X. Hua, X. Ji, J. He, J. H. Choi, and A. Khan, in *AVS 57th International Symposium* (Albuquerque, New Mexico, 2010).
[115]T. Chiarella, *et al*., Solid-State Electron. **54**, 855 (2010).
[116]L. Chang, Y.-K. Choi, D. Ha, P. Ranade, S. Xiong, J. Bokor, C. Hu, and T.-J. King, Proc. IEEE **91**, 1860 (2003).
[117]K. Ahmed and K. Schuegraf, IEEE Spectrum **48**, 50 (2011).
[118]K. Mistry, *et al*., Tech. Dig. - Int. Electron Devices Meet. **2007**, 247.
[119]C. Auth, *et al*., "45nm high-k+metal gate strain-enhanced transistors," VLSI Tech. Dig., 2008, pp. 128–129.